

Design and application of ion concentration polarization for preconcentrating charged analytes

Cite as: Phys. Fluids **33**, 051301 (2021); <https://doi.org/10.1063/5.0038914>

Submitted: 27 November 2020 • Accepted: 30 March 2021 • Published Online: 04 May 2021

 Majid Gholinejad,  Ali Jabari Moghadam,  Dinh-Tuan Phan, et al.



View Online



Export Citation



CrossMark

ARTICLES YOU MAY BE INTERESTED IN

[Multifactorial analysis of ion concentration polarization for microfluidic preconcentrating applications using response surface method](#)

[Physics of Fluids](#) **32**, 072012 (2020); <https://doi.org/10.1063/5.0010698>

[Ion concentration polarization on paper-based microfluidic devices and its application to preconcentrate dilute sample solutions](#)

[Biomicrofluidics](#) **9**, 014122 (2015); <https://doi.org/10.1063/1.4913366>

[Enhanced sample pre-concentration by ion concentration polarization on a paraffin coated converging microfluidic paper based analytical platform](#)

[Biomicrofluidics](#) **14**, 014103 (2020); <https://doi.org/10.1063/1.5133946>

[LEARN MORE](#)

APL Machine Learning

Open, quality research for the networking communities

COMING SOON



Design and application of ion concentration polarization for preconcentrating charged analytes

Cite as: Phys. Fluids 33, 051301 (2021); doi: 10.1063/5.0038914

Submitted: 27 November 2020 · Accepted: 30 March 2021 ·

Published Online: 4 May 2021



View Online



Export Citation



CrossMark

Majid Gholinejad,^{1,2,3,4} Ali Jabari Moghadam,^{4,a)} Dinh-Tuan Phan,⁵ Amir K. Miri,^{6,7} and Seyed Ali Mousavi Shaegh^{1,2,3,a)}

AFFILIATIONS

¹ Orthopedic Research Center, Mashhad University of Medical Sciences, P.O. Box 9187145785, Mashhad, Iran

² Clinical Research Unit, Ghaem Hospital, Mashhad University of Medical Sciences, P.O. Box 91735451, Mashhad, Iran

³ Laboratory of Microfluidics and Medical Microsystems, BuAli Research Institute, Mashhad University of Medical Sciences, P.O. Box 9196773117, Mashhad, Iran

⁴ Faculty of Mechanical Engineering, Shahrood University of Technology, P.O. Box 316, Shahrood, Iran

⁵ Institute for Nanobiotechnology, Johns Hopkins University, 3400 North Charles Street, Baltimore, Maryland 21218, USA

⁶ Biofabrication Lab, Department of Mechanical Engineering, Rowan University, Glassboro, New Jersey 08028, USA

⁷ School of Medical Engineering, Science, and Health, Rowan University, Camden, New Jersey 08103, USA

^{a)} Authors to whom correspondence should be addressed: Alijabari@shahroodut.ac.ir and Mousavisha@mums.ac.ir

ABSTRACT

Micro/nanofluidic devices integrated with ion concentration polarization (ICP) phenomenon have been used to preconcentrate low-abundant molecules for separation and detection purposes. This work reviews ICP-based devices focused on electrokinetic fundamentals of ICP in microfluidics and related design factors. We discuss various designs of ICP devices and then provide insight on the role of design factors in ICP function. In addition, fabrication methods and relevant materials for making ICP devices and nanojunctions are explained. This work provides the most up-to-date applications of ICP with emphasis on active and passive methods in controlling and stabilizing streams of preconcentrated molecules to enhance the separation and detection efficiency in diagnostics, desalination, and electrodialysis.

Published under license by AIP Publishing. <https://doi.org/10.1063/5.0038914>

I. INTRODUCTION

Electrokinetic-based methods,¹ such as isoelectric focusing² and electrophoretic,³ affinity-based extraction,⁴ and other methods^{5,6} have been realized for concentrating samples in microfluidic systems. Electrokinetic devices enable the continuous concentration of analytes.^{7–9} The ion concentration polarization (ICP) occurs at the interface of microchannels and charged nanometer-sized channels, where the exposure of ion-filled electrolytes to charged surfaces at *microscale* results in the adsorption of counterions. An electrical double layer (EDL) is formed over charged surfaces leading in fixed (stern) and diffusive layers [Fig. 1(a)]. Charged ions in diffusive layers may migrate when subjected to an external electric field, and this can sum up to a bulk transport of ions among electrodes. This physical phenomenon is known as electro-osmotic flow (EOF). At nanometer scales, overlapped EDLs allow counterion transport through nanochannels, thus triggering

an ion-selective behavior [Fig. 1(b)].¹⁰ The use of ion-selective nanochannels provides ICP for the separation of various targets. They were developed for analyte preconcentration in clinical diagnostics,^{1,11,12} filtration,¹³ desalination,^{14–18} nanofluidic diodes,^{19–21} and mixing purposes.^{22,23}

A. Ion concentration polarization (ICP) phenomenon

Integration of nanochannels or ion-selective membranes within microchannels is required to create ICP. The ion concentration gradient changes at micro–nanostructure interface under an electric field. Figure 2 illustrates the forces on co-ions, counterions, and negatively charged molecules under an electric field. Nanojunction/nanoporous membrane only allows counterions migration toward the cathode side (Fig. 2). This mechanism generates an ion enrichment zone at the

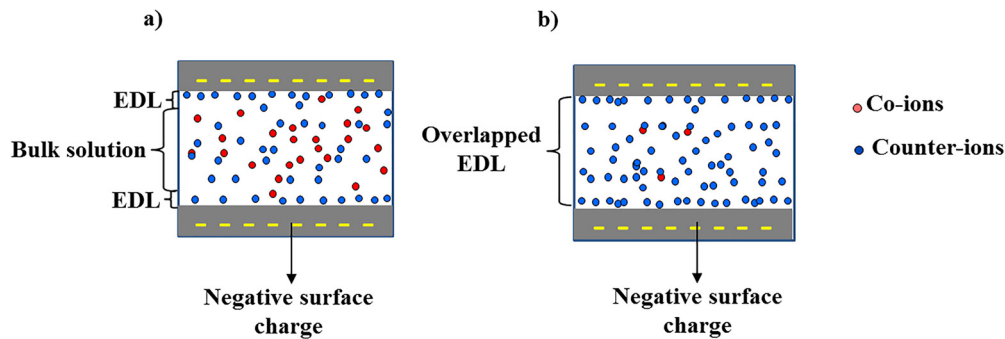


FIG. 1. (a) Schematics of a microchannel with electric double layers (EDLs), and (b) a nanochannel with overlapped EDLs.

cathodic side of the nanojunction. The efflux of counterions leads to the depletion of co-ions at the interface due to electrical neutrality and form an ion depletion zone. The depletion zone repels co-ions toward the anode side. Figure 3 presents a schematic of enrichment and depletion zones in a micro/nanofluidic device. The buffer solution with negatively charged molecules experiences electro-osmotic drag forces within the microchannel. As shown in Fig. 2, the electro-osmotic flow drives co-ions, counterions, and negatively charged molecules (bulk solution) toward the cathode (i.e., negative electrode) from left to right. On the other hand, the electrophoresis forces drive negatively charged molecules and co-ions toward the anode (i.e., positive electrode) in the opposite direction of EOF (from right to left) but the counterions are in the same direction as the bulk solution. The balances between these two opposing forces lead to preconcentrate the molecules at a certain location of the depletion boundary (Fig. 3).

The basis of ICP is the current–voltage response that primarily originates from the existence of ion depletion and enrichment zones. In region 1, known as the *Ohmic region*, the current increases linearly with the voltage. In this region, the resistance of the system remains constant and no ion depletion effect occurs (Fig. 4). After that, the depletion zone raises the electrostatic resistance, which leads to a plateau region of the current, known as the *limiting current regime*, and it is associated with the limited ion transport through the depletion

zone. Theoretical models suggest that the current in the circuit is saturated by the voltage exceeding the limiting regime. Experimental studies have shown that the increase in the voltage beyond the limiting regime results in a further increment of the current, known as the *over-limiting region*. Several different theories have been provided to explain the over-limiting behavior of ICP-based systems, including instability induced by the advection-diffusion balance of ions,²⁴ water molecule electrodialysis,^{25,26} or membrane surface conductivity.²⁷ Generally, the main cause of over-limiting is the electro-convection vortices and an extended space charge formation in the depletion zone. The formation of an extended space charge leads to the creation of a second kind electrokinetics and electro-osmotic instability.^{28–30}

II. FUNDAMENTALS AND GOVERNING EQUATIONS

We need to understand ion transport and electrokinetic forces mechanisms to have an efficient ICP design. Relevant governing parameters in the preconcentration process are buffer concentration, applied voltage, electrophoretic mobility, the surface charge of the microchannel, and the geometrical design of the device. Theoretical modeling can be employed to show the effect of such parameters. Solving Nernst Planck, Navier–Stokes, and Poisson equations can yield ionic concentration distribution (c), fluid velocity profile (\mathbf{u}), and electrical potential distribution (ϕ), which explain ICP characteristics. The

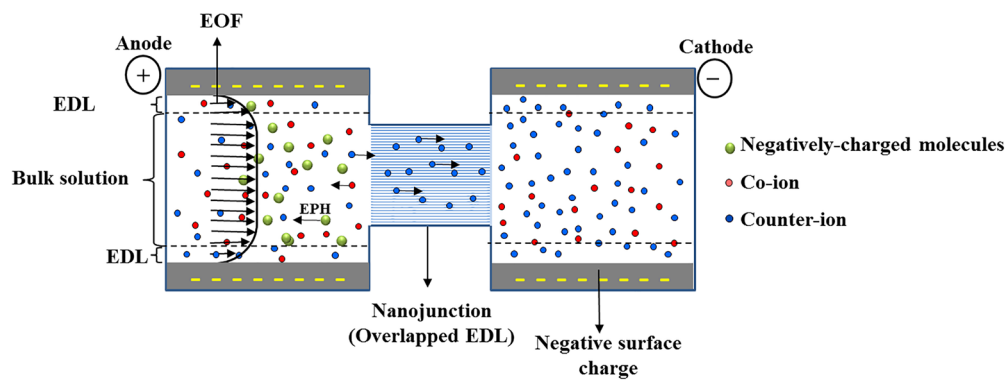


FIG. 2. Schematic of surface charged microchannel with negatively charged nanojunction and the forces (black arrows) applied on cocounterions and negatively charged molecules.

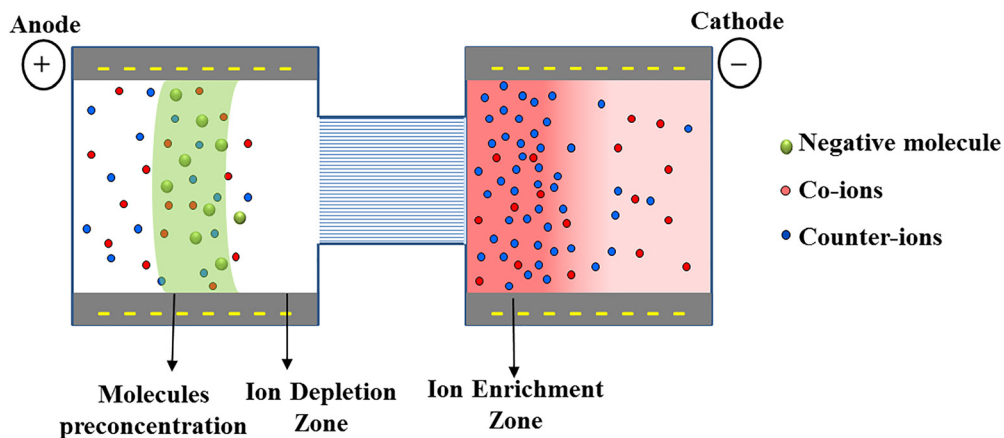


FIG. 3. Schematic of ICP enrichment, depletion, and preconcentrated zones under an applied voltage.

distribution of ion species concentration could be described by the Nernst–Planck equation³¹

$$\partial c_i(t)/\partial t = -\nabla \cdot \mathbf{J}_i, \quad (1)$$

where \mathbf{J}_i refers to the flux density of ion species

$$\mathbf{J}_i = - \left(\underbrace{D_i \nabla c_i(t)}_{\text{Diffusion}} + \underbrace{\mu_i z_i c_i(t) \nabla \phi(t)}_{\text{Electromigration}} \right) + \underbrace{c_i(t) \cdot \mathbf{u}(t)}_{\text{Convection}}, \quad (2)$$

where D_i , c_i , and z_i represent the diffusion coefficient of an ion species i , the concentration of an ion species i , and ionic species valence in an electrolyte solution, respectively. The flux density (\mathbf{J}_i) comprises diffusion, electromigration, and convection. The diffusion term is inversely related to the molecule size. The electromigration term is based on charged ions moving in the flow and the electrophoretic mobility of ions, which is shown by μ_i . It is related to the diffusivity defined by the Nernst–Einstein relation ($\mu_i \propto D_i$). The convection term is represented by the sample flow motion, i.e., the electro-osmotic flow.

Equation (1) reveals that to observe analyte preconcentration in a steady ICP device, i.e., $\partial c_i(t)/\partial t = 0$, a balance must be established between the fluxes of diffusion, electromigration, and convection of the tracer. Navier–Stokes and continuity equations define the fluid motion:

$$\nabla \cdot \mathbf{u} = 0, \quad (3)$$

$$\rho \frac{\partial \mathbf{u}(t)}{\partial t} + \rho(\mathbf{u} \cdot \nabla) \mathbf{u} = -\nabla p + \mu \nabla^2 \mathbf{u} - \rho_E \nabla \phi, \quad (4)$$

where ρ and μ are the density and dynamic viscosity of the solution, \mathbf{u} refers to the velocity vector, and p is the external hydrostatic pressure. The last term in Eq. (4), $\rho_E \nabla \phi$, indicates the net electrical body force exerted onto the fluid, which is related to an electrical field ($\mathbf{E} = -\nabla \phi$) and ion concentration. The ρ_E is the net charge density of the solution,

$$\rho_E = F \sum_i z_i c_i(t). \quad (5)$$

The Poisson equation relates electrical potentials to the ion concentration in the solution,

$$\nabla^2 \phi = -\frac{\rho_E}{\epsilon_0 \epsilon_r}, \quad (6)$$

where ϵ_0 and ϵ_r are vacuum permittivity constant and relative dielectric constants, respectively. Multiphysics simulations can be used to determine ionic concentration distributions, ionic currents, electric fields, flow fields such as vortex flows, and other parameters.^{32–37}

III. MATERIALS AND FABRICATION METHODS

Common substrate materials include polydimethylsiloxane (PDMS), silicon, glass, paper, and thermoplastics such as polymethyl methacrylate (PMMA). Photolithography and etching are conventional fabrication methods for microchannels in PDMS and silicon.³⁸ Complexity in the process and deformation of substrates during curing are the main drawbacks of these fabrication methods for ICP devices. Recently, cellulose paper has been recognized as an alternative substrate material for micro/nanofluidic applications. This paper is easier

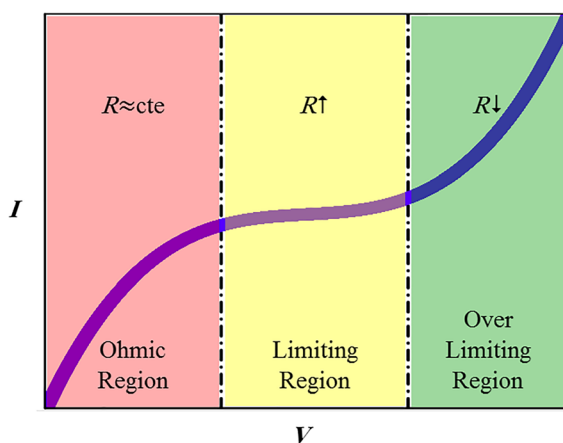


FIG. 4. Behavior of current–voltage in the Ohmic, limiting, and over-limiting regimes.

to fabricate and has a much lower cost compared to other substrates. It consists of cellulose fibers in which micrometer-sized gaps between the fibers induce liquid motion via capillary forces. A desired geometry can be patterned on cellulose paper by using a wax printing method³⁹ [Fig. 5(a)], electronic cutting,^{15,40,41} and direct spraying of the channels.⁴² Nonzero *zeta* potentials of cellulose surface in paper may induce electro-osmotic flows and this fact makes them appealing for electrokinetic devices.⁴³ Cellulose-matrix paper can be used to suppress the unwilling vortices generated near microchannel–nanochannel interfaces.⁴⁴ Following the preconcentration process, the accumulated analyte can be easily cut and separated from the device for further analysis.⁴⁵

Ion-selective nanochannels in ICP devices can be fabricated with various methods [Figs. 5(b-I)–5(b-IV)]. Nanofabrication is achieved through (i) the fabrication of planar⁴⁶ or vertical⁴⁷ nanochannels, (ii) nanoslits in a substrate such as silicon or glass,⁴⁸ (iii) or the integration of a nanoporous ion-selective membrane within the microfluidic structure of a device⁴⁹ using surface-patterned⁵⁰ or self-sealed nanoporous junction.⁵¹ The surface conductivity of the nanochannels determines ion transport properties and it is quantified by Dukhin number (*Du*), as the ratio of surface conductivity to bulk electrical conductivity of the fluid. Increased surface charge yields a lowered ionic strength of electrolytes (Dukhin number increases; *Du* > 1) and this leads to ion-selective behavior of nanochannels. The main drawback of nanochannels of the main substrate is the low surface charge (i.e., decreased perm-selectivity), in which ion-selectivity is hampered at high electrolyte concentrations (*Du* < 1).

Nanoporous membranes provide higher surface charges, thus they enhance perm-selectivity and compatibility of ICP devise with different substrates. Two examples of nanoporous membranes are the cation exchange membrane Nafion (DuPont, USA)^{15,52–55} and anion exchange membrane Fumasep® (FuMA-Tech GmbH, Germany).^{56,57}

Nafion is a sulfonated tetrafluoroethylene based fluoropolymer-copolymer that is widely used for the formation of ion-selective nanojunction in ICP devices. Nafion solution can be easily dropped at the desired location for nanojunction formation. Nanopores with negative surface charges are then formed in the presence of sulfonic acid group (HSO_3^-). Nafion membranes with different thicknesses can be inserted. Nafion nanopores have an average diameter of 6 nm that allows for the formation of overlapping EDLs for perm-selectivity.⁵⁰ It is also compatible with both polymeric and paper substrates, thus it has great potential for the fabrication of various ICP devices.⁵⁸

IV. DIFFERENT DESIGNS

For a better evaluation of ICP devices performance, they are categorized based on their designs.⁵⁹ The high voltage electrode is shown by V_H , and the low voltage electrode is represented by V_L (V_G : ground). Tangential electric field (E_t) is generated between V_H and V_L by an electro-osmotic flow while a normal electric field (E_n) is generated through potential difference between two ends of nanojunction.

A. H-shaped designs

H-shaped ICP devices include two microchannels, four electrodes, and an ion-selective membrane that connects the microchannels [Fig. 6(a)]. The sample channel is located between V_H and V_L , and it contains a sample solution. The electrodes of sample channels are connected to V_H and V_L , which create a tangential electrical field (E_t), and the electrodes of the buffer channel are electrically grounded (V_G). Under the effect of normal electrical field (E_N), only counterions of the nanojunction surface charge can pass through the nanochannel or membrane. This leads to ion depletion in the sample channel and ion enrichment in the buffer channel. The desired analytes are accumulated on the outer layer of the ion depletion zone. Various reported

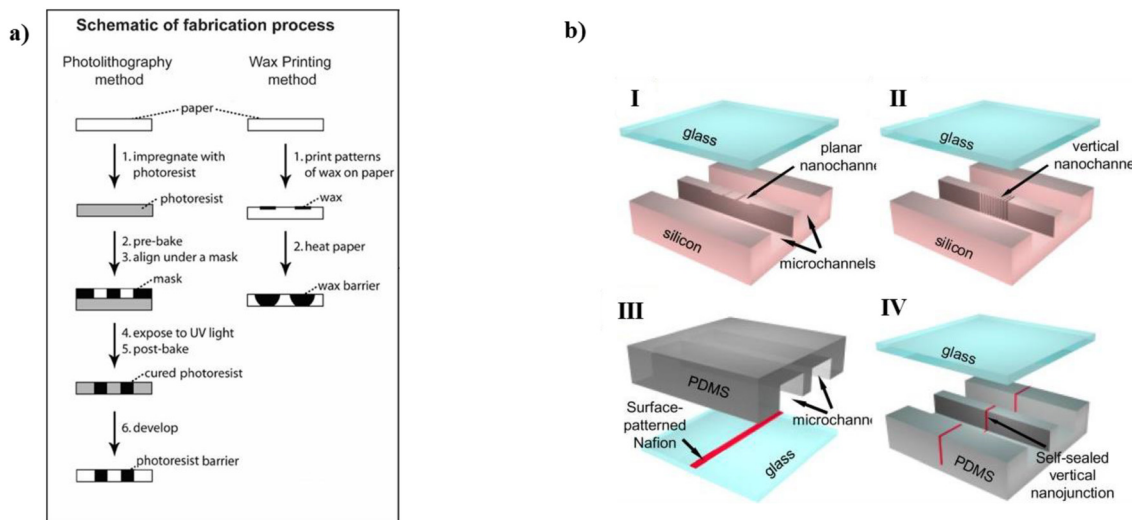


FIG. 5. (a) Schematics of the fabrication process for paper-based microfluidic systems using wax screen-printing method. Reprinted with permission from Martinez *et al.*, Anal. Chem. **82**, 3–10 (2010). Copyright 2009 American Chemical Society.³⁹ (b) Fabrication methods of perm-selective nanojunctions. Reprinted with permission from Kim *et al.*, Chem. Soc. Rev. **39**, 917 (2010). Copyright 2010 Royal Society of Chemistry.¹ (I) Planar nanochannel fabrication in Si/glass,⁴⁶ (II) vertical nanochannels in Si,⁴⁷ (III) surface-patterned Nafion junction,⁵⁰ and (IV) self-sealed Nafion junction.⁵¹

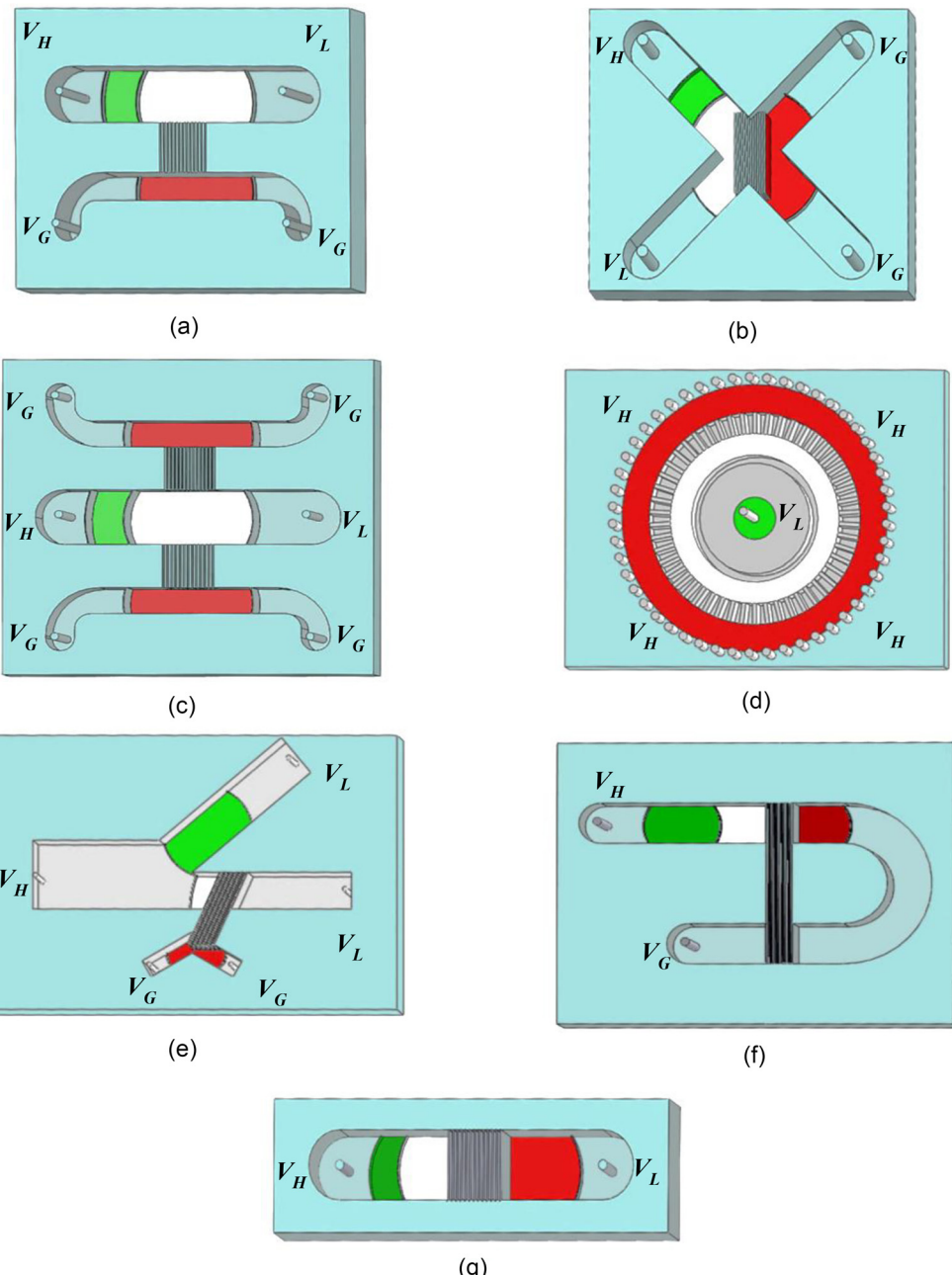


FIG. 6. Different designs of ICP-based preconcentration device for (a) H-shaped, reproduced after,⁶⁶ (b) X-shaped, reproduced after,⁷⁶ (c) dual-gate channel, reproduced after,⁸⁴ (d) O-shaped, reproduced after,⁹⁰ (e) Y-shaped, reproduced after,⁹⁷ (f) U-shaped, reproduced after,¹⁰¹ and (g) single channel, reproduced after.⁷³ White, red and green regions refer to ion depletion zone, ion enrichment zone, and preconcentrated molecules, respectively.

works on H-shaped devices are presented in Table I. The capacity of each device for preconcentrating an analyte of interest is evaluated by enrichment factor (*EF*) that is defined as the ratio of the final concentration of the analyte to its initial concentration.

The H-shaped ICP configuration has shown superiority to provide higher preconcentrations of analytes. The use of four electrodes is

the main limitation to voltage increase because of the occurrence of Joule heating. Gholinejad *et al.*⁷⁰ developed a statistical model via response surface method (RSM) to optimize H-shaped ICP system. They found that for a certain buffer concentration (~1 mM) an electric field of 20–30 V/cm is suitable to maximize preconcentration efficiency and avoid joule heating.

TABLE I. Reported experiments with their operating conditions for H-shaped design.

References	Microchannel	Nanojunction	Tracer	Tracer concentration	Voltage (V) or electric field	Enrichment factor (<i>EF</i>) (fold) at time (min)
Wang <i>et al.</i> ⁶⁰	Silicon wafers	Nanochannel	rGFP FITC-BSA (Fluorescein isothiocyanate-Bovine serum albumin) FITC dye	100 μM	$V_H = 10$ $V_L = 5$	10^7 at 40
Kim <i>et al.</i> ⁴⁴	NR ^a	Nanochannel	NR	10 μM	0–30	NR ^a
Kim <i>et al.</i> ⁵¹	PDMS	Nafion	BODIPY disulfonate β -phycoerythrin protein	0.1, 1, and 10 nM 1.67 and 16.7 pM	120	10^4 at 15
Kim <i>et al.</i> ⁶¹	PDMS	Nanochannel/Nafion	Fluorescein	1 $\mu\text{g}/\text{ml}$	3	NR ^a
Louér <i>et al.</i> ⁶²	Glass	Nanoslit	Fluorescein FITC-BSA	1.5 μM	80 V/cm	450 at 4.5
Chung <i>et al.</i> ⁶³	PDMS	Nanoslots	Fluorescence	5.8 nM	120	NR ^a
Song <i>et al.</i> ⁶⁴	PDMS	Nafion	Free DNA Bound DNA	5 nM–5 mM 25 nM	$\Delta V = 40, 60, 80$	500 at 3
Choi <i>et al.</i> ⁶⁵	PDMS	Nafion	Alexa Sulforhodamine B (SRB)	0.90 μM 24.14 nM	60–90	100 at 0.75
Nam <i>et al.</i> ⁶⁶	PDMS	Nafion	Fluorescent dye	10 mM	0.5–4	NR ^a
Gong <i>et al.</i> ⁶⁷	PDMS	Nafion	BSA protein ssDNA	1 $\mu\text{g}/\text{ml}$	$V_H = 30$ $V_L = 10$	NR ^a
Hong <i>et al.</i> ⁶⁸	PDMS	Nafion	Methylated DNA	500 fM–500 nM	100 V/cm	120 at NR ^a
Ngom <i>et al.</i> ⁶⁹	PMMA	Nanoslit	Ovalbumin	10 μM	10–50 V/cm	70 at 2

^aNR, not reported.

B. X-shaped designs

The configurations of X-shaped designs are very similar to the H-shaped ICP-based devices. X-shaped designs consist of V-shaped sample and buffer channels. The sample and buffer channels are connected through the nanojunction [Fig. 6(b)]. The voltage difference is applied to the sample channel and the buffer channel is connected to an electrical ground. As an electric field is applied between the high potential (V_H) and low potential (V_L), the electro-osmotic flow is generated on the sample channel. The sample channel develops ion depletion and ion enrichment zones which are created in the buffer channel. The negatively charged analytes are accumulated on the outer boundary of the ion depletion zone.

The ICP in X-shaped devices is highly sensitive to voltage amplitude. If the voltage exceeds a certain threshold, the preconcentration plug created in the ion depletion boundary may disappear⁷¹ [Fig. 7(a)]. Higher voltages produce a large velocity gradient in the V-shaped sample channel, generating vortices near the ion depletion zone [Fig. 7(b)]. The formation of vortices around the depletion zone in X-shape structures had been investigated both experimentally and numerically.^{34,72,73} Various reported works on X-shaped devices are presented in Table II.

C. Dual-gate channel designs

A dual-gate channel consists of one sample and two buffer channels that are connected together through a nanojunction [Fig. 6(c)].

The tangential electric field (E_T) is generated across the sample channel from left to right, and the normal electric field (E_N) moves toward buffer channels. Ion depletion zone is created adjacent to the nanojunction in the sample channel and the negatively charged analytes are accumulated at the outer boundaries of the depletion zone. The nanojunction characteristic is a crucial design parameter for the dual-gate geometry. Therefore, it can be estimated that chooses an appropriate nanojunction, e.g., using high surface charged material, is absolutely essential to achieve higher performance. The experiments on a dual-gate channel and H-shaped device demonstrate the ability of the dual gate channel for the same operating conditions.^{51,77,78} Table III shows studies on the dual gate channel devices.

D. O-shaped designs

The O-shaped structure or radial preconcentration is a new design of ICP devices (Table IV). In this approach, the nanojunction is placed on a constant radius (O-shape) to concentrate the analytes radially [Fig. 6(d)]. As shown in Fig. 6(d), the sample is injected vertically into the middle of the sample channel surrounded by the membranes. Once voltage is applied, a radial ion depletion zone is created near the cathodic side of the membrane and an ion enrichment zone appears at the anodic side. The ion depletion zone is propagated toward the center of the channel leading to a concentration of the molecules at the interface of the depletion zone. The concentrated analytes then enter the middle sample channel.

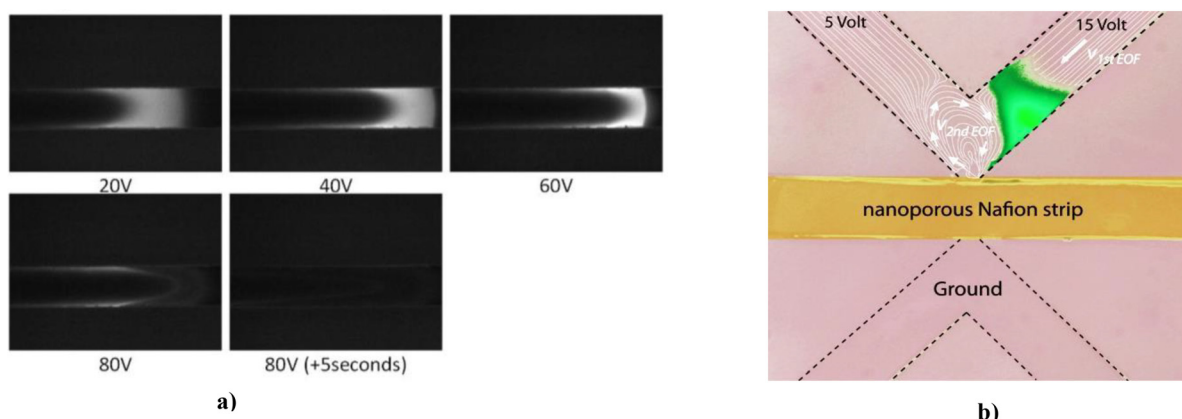


FIG. 7. (a) The preconcentration plug disappears by increasing voltage for $10 \mu\text{M}$ fluorescein mixed with 10 mM KCl in X-shaped design. Reproduced with permission from Yuan *et al.*, *Anal. Chem.* **87**, 8695–8701 (2015). Copyright 2015 American Chemical Society.⁷¹ (b) Generated vortices around the ion depletion zone in the V-shaped sample channel. Reproduced with permission from Shen *et al.*, *Anal. Chem.* **82**, 9989–9997 (2010). Copyright 2010 American Chemical Society.⁷⁵

TABLE II. Reported experiments with their operating conditions for X-shaped design.

References	Microchannel	Nanojunction	Tracer	Tracer concentration	Voltage (V) or electric field	EF (fold) at time (min)
Kim <i>et al.</i> ⁴⁹	Glass/PDMS	Nanochannel	FITC-BSA	100 nM–1 pM	$V_H=200$ $V_L=200$	10^3 – 10^6 at 30
Yu <i>et al.</i> ⁷⁴	PDMS	Nanofissures	Ovalbumin FITC-DSA	100 pM	$V_H=80$ $V_L=80$	10^3 – 10^5 at 10
Shen <i>et al.</i> ⁷⁵	PDMS	Nafion strip	AF-BSA	60 pM 6 nM 60 nM	$V_H=15$ $V_L=5$	2×10^4 at 7
Kim and Kim ⁷⁶	PDMS	Nafion	FITC labeled BSA	5 nM	$V_H=60$	10^3 at 10
Yuan <i>et al.</i> ⁷¹	Glass/Tape	Nafion strip	Fluorescein sodium	1 and $10 \mu\text{M}$	$V_L=30$ 0–200	5000 at 5
Hailong <i>et al.</i> ⁷²	PDMS	Nafion (CEM&AEM)	Fluorescein sodium salt Rhodamine 6G	100 μM	$V_H=20$	$V_L=8$ 40 at 10

E. Y-shaped designs

Y-shaped designs mainly consist of a Y-shaped sample channel interconnected with a buffer channel as shown in Fig. 6(e). The sample is loaded into the sample channel to pass through the nanoporous membrane inserted at the junction of the sample channel. A voltage is applied to the sample channel, while the buffer channel is kept electrically grounded. Charged analytes are repelled from the ion depletion zone and directed to the upper side of the sample channel (Table V). The Y-shaped designs are commonly used for water desalination devices^{14,17,18} and biomolecule separation devices.^{91–94} Water flows into the main channel and when ICP is triggered, brines are accumulated on the upper side of the Y-shaped sample channel, while the desalted water moves through the sample channel.

As reported in the previous experiments, the width of the upper side of the Y-shaped sample channel should be shorter than the main sample channel to improve the enrichment factor.⁹⁸ Kwak *et al.*⁹⁸ also

claimed that by controlling hydrodynamic resistance of the main and concentrated channel, the enrichment factor can be adjusted.

F. U-shaped designs

U-shaped designs have been developed to decrease the number of employed electrodes. In a U-shaped structure, there is only one sample channel and the buffer channel is eliminated. The nanojunction is interconnected to the U-turn sample channel, Fig. 6(f). The voltage is applied only to one side of the sample channel and the other side is kept electrically grounded. The ion depletion zone is created adjacent to the nanojunction and repelled analytes are accumulated at the outer layer of ion depletion zone (Table VI).

The entrance length of sample channel is critical to achieve efficient preconcentration in U-shaped design. Ko *et al.*⁹⁹ reported that the effect of the normal electric field (E_N) on preconcentration process

TABLE III. Reported experiments with their operating conditions for dual gate channel design.

References	Microchannel	Nanojunction	Tracer	Tracer concentration	Voltage (V) or electric field	EF (fold) at time (min)
Dai <i>et al.</i> ⁷⁹	PDMS	PETE (Polyester Track Etched)	Fluorescein DNA	10 µg/ml	100	800 at 5
Foote <i>et al.</i> ⁸⁰	Glass coated with PDMA (poly dimethylacrylamide)	Porous silica	Fluorescently labeled proteins	(10 nM) 50 mM	340 V/cm	600 at 8
Kim <i>et al.</i> ⁵¹	PDMS	Nafion	BODIPY disulfonate β-phyceroylthrin protein	0.1, 1, and 10 nM 1.67 nM and 16.7 pM	120	10 ⁴ at 15
Lee <i>et al.</i> ⁵⁰	PDMS	Nafion	β-phyceroylthrin protein	40 pM–40 nM	$V_H = 50$ $V_L = 25$	5×10^4 at 5
Chun <i>et al.</i> ⁸¹	PDMS	Poly-AMPS	TRITCalbumin Rhodamine 6G Fluorescein	1 µM 30 µM 50 µM	$V_H = 60$ $V_L = 45$	400 at 8
Chang <i>et al.</i> ⁴⁸	Soda-lime glass	Nanochannel	NR ^a	1 mM	0–30	NR ^a
Jen <i>et al.</i> ⁸²	PDMS	Nanofracture	FITC-BSA	1 and 100 nM	50	1.56×10^4 at 60
Syed <i>et al.</i> ⁸³	PDMS	Colloidal-silica	Cy5 DNA β-phyceroylthrin protein	10 nM 4 µg/ml	$V_H = 30$ $V_L = 25$	1700 at 15 100 at 15
Ouyang <i>et al.</i> ⁸⁴	PDMS	Nafion resin	NR ^a	0.1 nM	0.512	NR ^a

^aNR, not reported.**TABLE IV.** Reported experiments with their operating conditions for O-shaped design.

References	Microchannel	Nanojunction	Tracer	Tracer concentration	Voltage (V) or electric field	EF (fold) at time (min)
Scarff <i>et al.</i> ⁸⁵	PDMS	Nafion	FITC-BSA	250 nM	200	168 at 0.5
Aïzel <i>et al.</i> ⁸⁶	Silicon wafer	Nanochannel	Fluorescein	NR ^a	100	100 at 20
Aïzel <i>et al.</i> ⁸⁷	Silicon wafer	Nanochannel	Polystyrene nanobeads	50 nM	50	800 at 60
Gong <i>et al.</i> ⁸⁸	PMMA	Nafion	Fluorescein	10 mM	50	40 at 2.5
Lee <i>et al.</i> ⁸⁹	PDMS	Nafion	Sulforhodamine B (SRB)	50 nM	15	10 at 1
Lee <i>et al.</i> ⁹⁰	PDMS	Nafion	Alexa 488 DsDNA Polystyrene	30 µl 30 µl 1 µm	10	10 at 90

^aNR, not reported.**TABLE V.** Reported experiments with their operating conditions for Y-shaped design.

References	Microchannel	Nanojunction	Tracer	Tracer concentration	Voltage (V) or electric field	EF (fold) at time (min)
Phan <i>et al.</i> ⁹⁵	PDMS	Nafion	Fluorescein sodium salt	10 µM	100 V/cm	50 at 2
Hong <i>et al.</i> ⁹⁶	Paper	Nafion	Alexa Fluor 488	15.15 µM	100	30 at 10
Phan <i>et al.</i> ⁹²	PDMS	Nafion	Fluorescein sodium salt	1 µg/ml	0.1	500 at 10
Berzina and Anand ⁹⁷	PDMS	Nafion	Dye-linked albumin	0.05 mg/ml	0–55	20 at NR ^a

^aNR, not reported.

could be neglected for the U-shaped configuration. Thus, the enrichment factor is mainly dependent on E_T , which can be controlled by adjusting the length of sample channel.

G. Single channel design

Continuous enhancement of ICP-based devices to obtain a simple yet functional design has led to the development of single-channel

TABLE VI. Reported experiments with their operating conditions for U-shaped design.

References	Microchannel	Nanojunction	Tracer	Tracer concentration	Voltage (V) or electric field	EF (fold) at time (min)
Ko <i>et al.</i> ⁹⁹	PDMS	Nafion	Fluorescein	0.01, 0.1, and 1 $\mu\text{g}/\text{ml}$	50–100	4000 at 30
Chen <i>et al.</i> ¹⁰⁰	PDMS	Nafion	Fluorescein	1 μM and 100 nM	50	200 at 2.5
Chao <i>et al.</i> ¹⁰¹	PDMS	Nafion	Fluorescein	0.1 μM	200 V/cm	400 at 6
			FITC-BSA	1 μM		

ICP (SC-ICP) devices. Single-channel design mainly comprises of a single channel and a pair of electrodes located at the ends of a microchannel. The nanoporous membrane is located on the bottom of the microchannel, usually at the middle of the channel [Fig. 6(g)]. Once voltage is applied, the sample moves from higher voltage to lower voltage due to EOF. The nanojunction repels analytes, and the enrichment and depletion zones are formed. This configuration could be easily fabricated in a cost-effective manner. Table VII shows that this design has been widely implemented in cellulose paper-based substrates.

Wei *et al.*¹⁰² improved the concentration performance of SC channel design via enhancing the thickness of ion-selective membrane. Wang and Yang¹⁰³ enhanced the nanojunction conductivity (σ_n) by

adding graphene-oxide (GO) to Nafion. The results revealed that GO-Nafion could improve the preconcentrating rate and enhance the enrichment factor. It can be seen that the results of the conducted experimental methods in the literature boost the preconcentration efficiency.

V. RECENT DEVELOPMENTS

Various strategies have been developed to enhance the enrichment factor such as throughput of isolation and sample processing. The integration of actuation mechanisms like parallelization, the converging the sample channel, or valving with ICP devices to facilitate on-chip liquid handling.

TABLE VII. Reported experiments with their operating conditions for SC channel design.

References	Microchannel	Membrane	Tracer	Tracer concentration	Voltage (V) or electric field	EF (fold) at time (min)
Dhopeshwarkar <i>et al.</i> ¹⁰⁴	PDMS	Hydrogel	Fluorescein	5 μM	100	100 at 2
Ku <i>et al.</i> ¹²	PDMS	Nafion	C-reactive protein (CRP)	10 ng/ml	40	500 at NR ^a
			FITC			
Kim <i>et al.</i> ⁷³	PDMS	Nafion	FITC	1–100 nM	50	10^4 – 10^6 at 60
			Rhodamine 6G			
			Rhodamine 110			
Quist <i>et al.</i> ¹⁰⁵	PDMS	Nanochannel	Fluorescein	200 nM	95 and 200	1000 at 4.5
Gong <i>et al.</i> ¹⁰⁶	Cellulose paper	Nafion	Fluorescein	2 μM	200 V/cm	150 copies/mL at NR ^a
			Calcein	1 μM		
Yang <i>et al.</i> ¹⁰⁷	Cellulose paper	Nafion	Fluorescein	10^{-5} M	50	20 at 2
			FITC-BSA			
Kwak <i>et al.</i> ¹⁰⁸	PDMS	Nafion	Alexa Fluor 488	1–100 mM	0.5–100	10^4 at 10
Liu <i>et al.</i> ⁴¹	Cellulose paper	Nafion	FITC	10 μM	140	28 at 1
Phan <i>et al.</i> ¹⁵	Cellulose paper	Nafion	Fluorescein sodium salt	80 mM	50–100	60 at 2.5
Yeh <i>et al.</i> ¹⁰⁹	Cellulose paper	Nafion	Fluorescein	10^{-8} M	0–210	944 at 28
			FITC-BSA			
Lee <i>et al.</i> ¹¹⁰	PDMS	Nafion	Lipid vesicles	1 mg	25–100	160 at 10
Son <i>et al.</i> ⁴⁵	Cellulose paper	Nafion	Alexa Fluor 488	10 mM	50	40 at 1
Liu <i>et al.</i> ¹¹¹	Sartorius filter paper	Nafion	FITC	10^{-5} M	50	100 at 4
Gao <i>et al.</i> ¹¹²	Paper	Nafion	Methylated DNA (GSTP1 and EFEMP1)	500 fM–500 nM	100 V/cm	120 at NR ^a
Perera <i>et al.</i> ¹¹³	Paper	Nafion	Escherichia coli with SYTO 9	20 μM	50–90	2×10^5 at 20
Perera <i>et al.</i> ⁴⁰	Paper	Nafion	Fluorescein sodium salt	40 μM	100	2000 at 10
Liu <i>et al.</i> ⁴¹	Paper	Nafion	FITC	20 mM	50	220 at 0.66
Liu <i>et al.</i> ⁴²	Paper	Nafion	FITC	5 mM	50	100 at 4

^aNR, not reported.

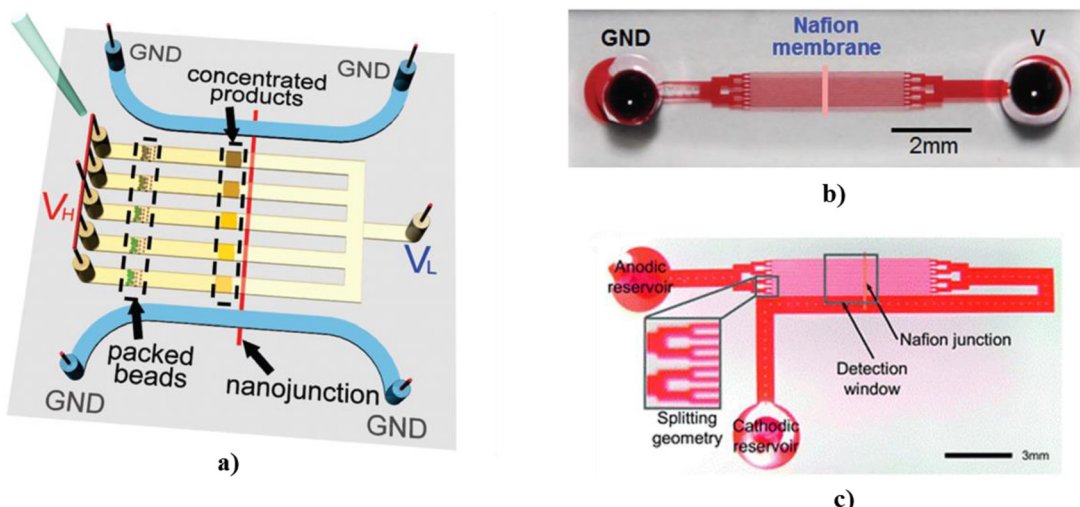


FIG. 8. Parallel ICP concentrator (a) dual-gated channel. Reprinted with permission from Cheow *et al.*, *Anal. Chem.* **82**, 3384 (2010). Copyright 2010 American Chemical Society.¹¹⁴ (b) Single channel. Reproduced with permission from Ko *et al.*, *Lab Chip* **12**, 4476 (2012). Copyright 2012 Royal Society of Chemistry.¹¹² (c) U-shaped. Reprinted with permission from Ko *et al.*, *Lab Chip* **11**, 1353 (2011). Copyright 2011 Royal Society of Chemistry.⁹⁹

A. Parallelization of sample channels

To enhance the capacity of the ICP devices to process higher samples volumes, i.e., high-throughput performance, the parallelization of microchannels has been developed. To this end, a series of sample channels has been applied to different designs of ICP devices including dual-gate,^{50,114} U-shaped,^{99,115} and single channels,¹² Fig. 8. As reported in the literature, the sample channels have been parallelized from 5 to 126.^{99,114} The concentration speed in each sample channel is controlled by both the normal electric field through controlling the width of micro/nanochannel and the tangential electric field through controlling the length of microchannels.¹¹⁵ Thus, in such devices the distance between sample channels and the length of sample channel must be considered within an appropriate range to achieve maximum efficiency.

B. Converged shape sample channel

To achieve a higher and faster preconcentration process compared to straight channels, converged channel geometry for sample channel has been tried for U-shaped^{100,116} and SC-ICP devices.¹⁰⁷ The results show that the converged channel could compact the charged analytes and enhance the enrichment factor. On the other hand, Yang *et al.*¹⁰⁷ pointed out that reducing the channel width could reduce the nanojunction role with subsequent effect on decreasing the overall ICP performance. Also, Kovář *et al.*¹¹⁷ found that the converged channel, or diverged channel, did not significantly affect the preconcentration of fluorescein.

The reason beyond this disparity is that converging the geometry of the sample channel decrease the channel conductance; however, the electro-osmotic velocity should be considered as well.¹¹⁸ The electro-osmotic velocity enhances with increased applied potential along the microchannel in the converged channel. As a result, a compromise among converging sample channel, nanojunction thickness and electro-osmotic velocity should be considered to enhance the ICP performance.

C. Controlling the location of concentrated analytes plug

The analysis of ICP-based devices reveals that in some cases, the zone of concentrated analytes, located at the outer boundary of the ion depletion region, losses its stability and begins to propagate along its adjacent microchannel.^{119–122} Such propagation could negatively affect the device operation by increasing the process time, decreasing the enrichment factor, and even fading the concentrated analyte plug. Thus, it is desirable to limit the movement of preconcentrated plug. The propagation of the concentrated analytes mainly occurs due to the electro-osmotic instability in the overlimiting region. Thus, strong vortices generated by the amplified electric field in the ion depletion zone distort the concentrated plug. This section discusses the active and passive techniques applied to ICP devices to diminish unwilling instability and pinpoint the concentrated charged analytes at the desired positions.

1. Passive methods

Passive methods include manipulating the movement of a pre-concentrated plug with no use of external source. This approach could be mainly realized through modifying the structure of ICP-based devices. Experimental studies show that modulation of geometry and the implementation of fins inside sample channel allows for controlling instabilities in ICP devices in a passive fashion.

a. Device configuration. Decreasing the microchannel depth to suppress generated vortices inside the depletion region provides a simple method to improve the stability of formed plug.⁴⁴ Choi *et al.*⁶⁵ reported another method to confine vortices in microchambers with the goal of stabilizing the preconcentrated analyte. In this case, by implementing microchambers the vortices are trapped in the chambers and improved the stability of the device.

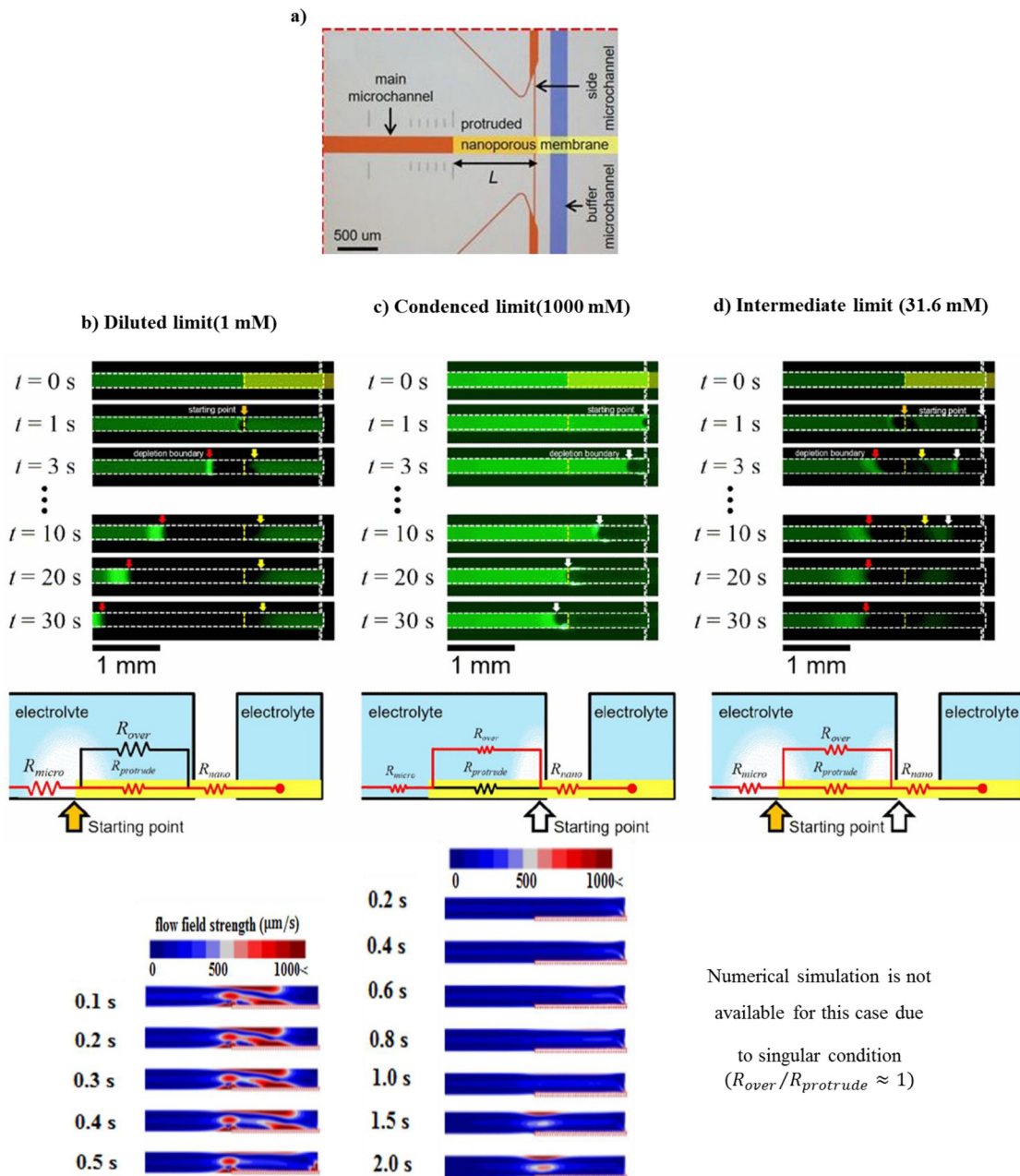


FIG. 9. Experimental, equivalent circuit, and numerical results of propagating ion depletion zone for (a) device configuration. L is the length of protruded nanoporous membrane from the main microchannel. Schematics of Dilute limit (1 mM), (b) condensed limit (1 M), and (c) intermediate (31.6 mM). Reprinted with permission from Kim *et al.*, Sci. Rep. 7, 5091 (2017). Copyright 2017 Author(s), licensed under a Creative Commons Attribution 4.0 License.¹²³

Kim *et al.*¹²³ protruded Nafion membrane along the sample channel to diminish instability in the ion depletion zone, Fig. 9(a). They investigated different electrolyte concentrations, 1 mM for diluted limit, 1000 mM for condensed limit, and 31.6 mM for intermediate regime, Figs. 9(b)–9(d). Their numerical and experimental analyses confirmed that strong electrokinetic instability could be

considerably suppressed by using a protruded membrane, especially in the condensed limit.

Kwak *et al.*¹⁰⁸ used two line-patterned Nafion membranes to confine the preconcentrated analytes between membranes, Fig. 10(a). Unlike common ICP-based devices, in this case, two ion depletion zones are merged and confine the preconcentrated analytes between

Numerical simulation is not available for this case due to singular condition ($R_{\text{over}}/R_{\text{protrude}} \approx 1$)

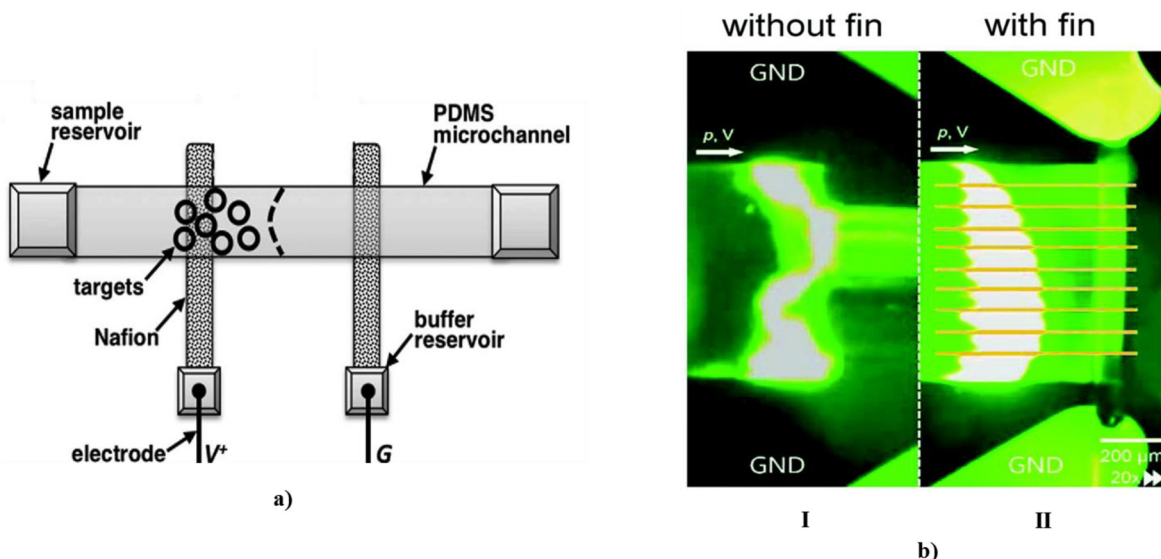


FIG. 10. (a) Schematics of a spatiotemporally defined preconcentrator using two Nafion strips Reproduced with permission from Kwak *et al.*, Anal. Chem. **88**, 988 (2015). Copyright 2015 American Chemical Society.¹⁰⁸ (b) Preconcentration of fluorescent dye: (I) without microfin and (II) with microfin. Reproduced with permission from Kim *et al.*, Nanoscale. **9**, 3466–3475 (2017). Copyright 2017 Royal Society of Chemistry.

the membranes. This method stabilizes the preconcentrated fluorescent dyes using a wide range of voltage (0.5 – 100 V), ionic strength (1 – 100 mM KCl), and pH (3.7 – 10.3).

b. Fin implementation. The implementation of a fin inside the sample channel provides another passive method used in Dual gate¹²⁴ and O-shaped¹²⁵ ICP devices. Kim *et al.*¹²⁴ declared that a

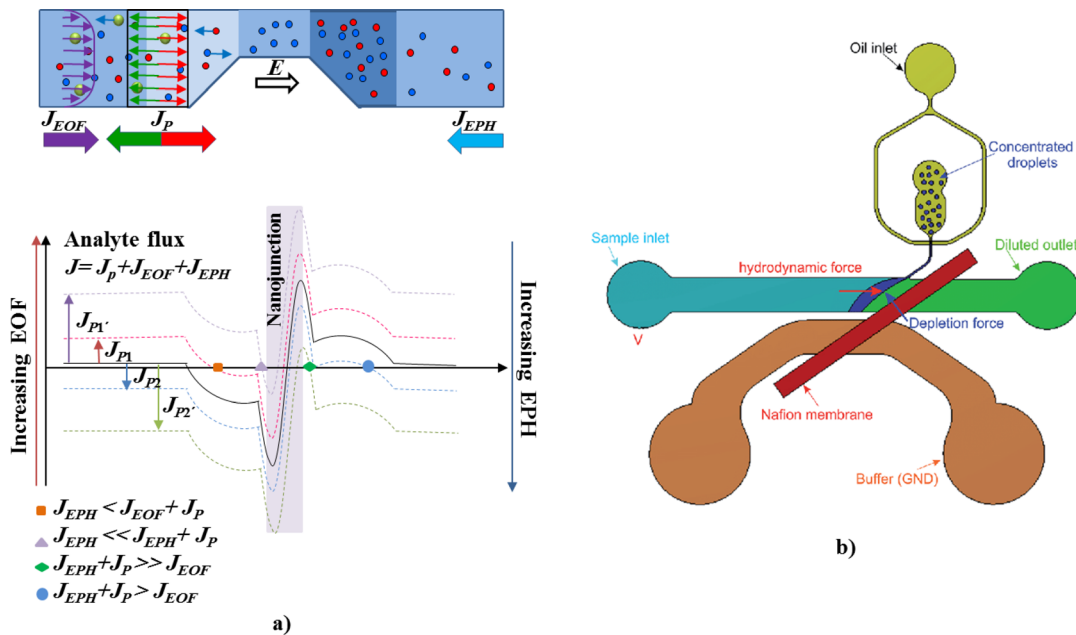


FIG. 11. (a) Mechanism of pressure-assisted preconcentration and separation. Reprinted with permission from Louér *et al.*, Anal. Chem. **85**, 7950 (2013). Copyright 2013 American Chemical Society.⁵² (b) Combination of a continuous-flow concentrator and a droplet generator. Reprinted with permission from Phan *et al.*, RSC Adv. **5**, 443367 (2015). Copyright 2015 Royal Society of Chemistry.

channel without a fin experienced multiple vortices near the ion depletion zone, Fig. 10(b-I). However, the use of a fin contributed to stable accumulation of concentrated plug, Fig. 10(b-II).

2. Active methods

As discussed in Sec. II, to boost the efficiency of preconcentration process, a balance must be accomplished between the forces applied on charged analytes.¹⁰⁸ Active methods employ external power sources to aid ICP-based devices. These methods confine the location of the concentrated plug and therefore maintain the balance. Section VC2 (a–c) discusses various reported active methods.

a. Pressure difference. An active method to maintain the balance of forces on charged analytes is to apply a pressure difference along the sample channel. Louér *et al.*⁶² investigated the effect of hydrodynamic pressure ($\Delta p = 0.9$ bar) in the same and opposite directions of the EOF ($\Delta E = 80$ V/cm) to control the preconcentrated plug, Fig. 11(a). In both directions, the locations of BSA concentrated plugs remained stable. The use of pressure difference in SC-ICP was also reported by Lee *et al.*¹²⁵ They claimed that the addition of hydrodynamic pressure could diminish a generated vortex. Also Kwak *et al.*⁹⁸ demonstrated that a continuous-flow biomolecule and cell concentrator applied an electric field and pressure field. They tested various geometries of the device including width and length with diverse samples at different buffer electrolyte concentrations. The results show that by balancing hydrodynamic pressure, the enrichment factor could vary from 1 to 200. Recently, Ngom *et al.*⁶⁹ investigated the effects of the electric field and counter pressure to find a stable preconcentrating regime. The experimental studies revealed that for ovalbumin (10 μM) the stable preconcentrating regime exists at both low electric field ($E < 20$ V/cm) and low counter pressure ($p < 0.4$ bar). On the other hand, Kim *et al.*⁵¹ observed that the preconcentrating plug lost its stability over time by applying an external pressure. This is inconsistent with the findings reported by Louér *et al.*⁶² and Lee *et al.*¹²⁵ To stabilize the preconcentration analytes using an external pressure, it is essential to understand the pressure range and its gradient direction, as well as microchannel geometry. It can be predicted that when the convection forces in Eq. (2) are weak, applying pressure difference could be used as supplementary driven flow to balance the forces exerted on molecules.

b. Droplet generator. Phan *et al.*⁵³ proposed an H-shaped ICP device integrated with a droplet generator, Fig. 11(b). Once an electric field is applied, a preconcentrated plug could be fixed at a certain position based on the balance between the depletion force in ICP and hydrodynamic forces generated by the input pressure and the backflow from the droplet generator. The concentration of a droplet's content can be tuned with a combination of flow rates and applied voltages. To make a demonstration of this application for biological analysis, the continuous flow droplet-based concentrator using ICP can be integrated with a droplet generator in which the concentration of droplets can be programmable and generated in a desired sequence.¹²⁶

c. Microheater. Inserting microheaters along microchannel is another active control method proposed by Park and Yossifon,¹²⁷ Fig. 12(a). A combination of an electric field and temperature gradient by microheaters can generate electrothermal flow, which could control the propagation of the depletion layer, Fig. 12(b). On the other hand, once microheaters are off, the propagation of depletion zone drives analytes away from the concentration zone, which is dispersed in the depletion zone.

D. Simultaneous preconcentration and separation

Recently, more attention has been paid to the simultaneous preconcentration and separation of multiple analytes in a single device. As each analyte has a unique electrophoretic mobility, multiple analytes could be separated by a specific electric field. The separation resolution (SR), which is defined as the ratio of distance and width of two adjacent preconcentrated bands, is used to quantify the separation efficiency.

Song *et al.*⁶⁴ presented an “H-shape” ICP device for concurrent preconcentration and separation of free biotinylated DNA molecules and bound DNA molecules, i.e., biotinylated DNA with streptavidin bound. At the beginning of ICP process ($t = 0$ –60 s), it was impossible to distinguish free biotinylated DNA from bound DNA bands, whereas a distinct separation could be observed at $t = 240$ s, Fig. 13(a). A separation resolution of 1.85 was obtained, which is higher than the value reported by other methods such as field amplified sample stacking technique ($SR = 1.4$).¹²⁸ In another study, the same research group investigated the effect of using a bipolar

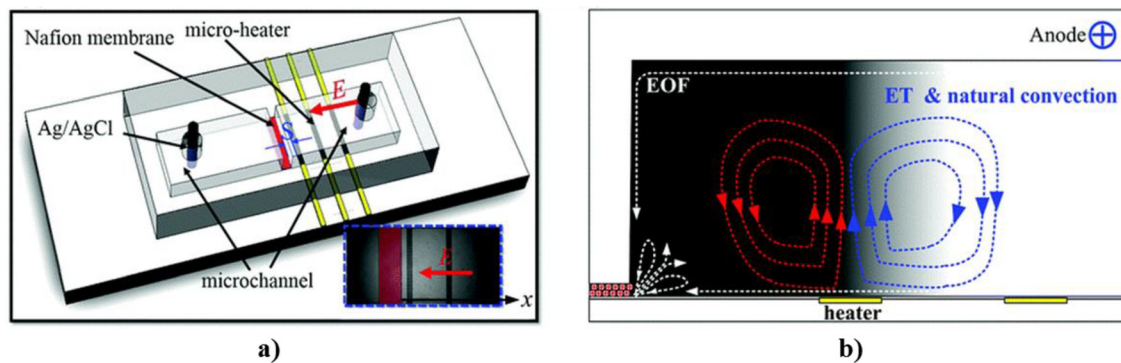


FIG. 12. (a) A schematic of the microchannel–Nafion membrane device with an embedded array of microheaters. (b) A schematic illustration of the suppression of diffusion layer propagation by the induced ET flow and natural convection. Reprinted with permission from Park and Yossifon, *Nanoscale* **10**, 11634 (2018). Copyright 2018 Royal Society of Chemistry.¹²⁷

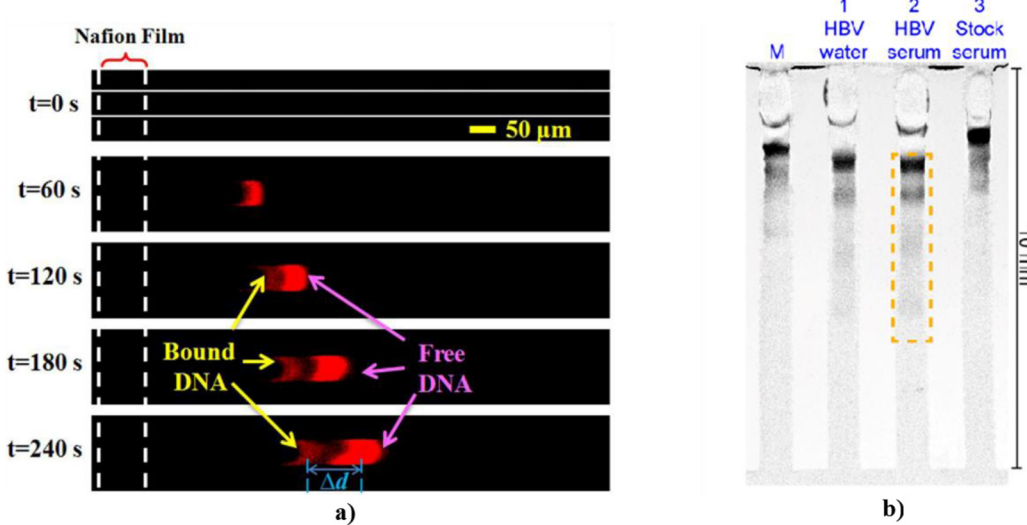


FIG. 13. (a) Concurrent concentration and separation of the free and bound biotinylated DNAs. The free DNA consists of biotinylated 102-mer DNA, whereas the bound DNA consists of streptavidin bound to the biotin end. Reprinted with permission from Song *et al.*, *Microfluid. Nanofluid.* **17**, 697 (2014). Copyright 2014 Springer-Verlag, Berlin Heidelberg.⁶⁴ (b) Multiplexed analysis of the DNA standard, HBV DNA in water, HBV DNA in serum, and stock serum in a multichannel device. Reproduced with permission from Gong *et al.*, *J. Am. Chem. Soc.* **137**, 13917 (2015). Copyright 2015 American Chemical Society.¹⁰⁶

electrode.¹²⁹ Under identical operating conditions, a maximum separation resolution of 1.5 was achieved, which demonstrated the importance of Nafion film ($SR = 1.85$) for both preconcentration and separation mechanisms.

Gong *et al.*¹⁰⁶ studied the separation and detection of hepatitis B virus (HBV) DNA fragments, i.e., precore, core, surface, X, and polymerase, in a multichannel ICP device, Fig. 13(b). The separation resolutions in all four channels ranged from 0.5 to 0.7, which is low compared to other studies. The proposed device could be used to

consistently detect the surface and precore regions, but the device failed to distinguish X and core regions of the HBV genome, which is necessary for the identification of hepatitis B.

Lee *et al.*¹³⁰ presented an H-shaped device to preconcentrate and separate free and dCas9-DNA, simultaneously. As shown in Fig. 14, free DNA molecules propagated during time steps, however, dCas9-DNA were stacked. It was found that once the electrophoretic mobility is higher than the critical electrophoretic mobility ($\mu_{cr} = 2.7 \times 10^{-8} \text{ m}^2/\text{V s}$ in their case), free DNA molecules start to propagate. But the dCas9-DNA with lower electrophoretic mobility than critical electrophoretic mobility are stacked in a fixed position near nanojunction.

Baek *et al.*¹³¹ proposed driftless preconcentration leveraged by convection and diffusion using an H-shaped ICP device. In this study, they focused on the dynamic behavior of preconcentration/separation of analytes, especially driftless migration, where the applied electric field is orthogonal to the direction of the drift migration. According to their analytical and experimental studies, the ratio of convection to diffusion had a critical impact on the shape of preconcentrated/separated analytes. They found that analytes could be accumulated uniformly along the channel in a plug shape once strong diffusion regime exists. However, analytes would be accumulated on top and bottom of the microchannel with a dumbbell shape, once weak diffusion regime occurs. More details of the driftless preconcentration could be found in Choi *et al.*¹³² works.

Berzina and Anand⁹⁷ studied the separation of albumin from blood plasma using a Y-shaped ICP-based system. By investigating the effects of a driving voltage (5.0–55.0 V) and flow rate (5.0–70 nl/min) on separation efficiency, which as derived from the percentage of decrease in the concentration of dye-linked albumin, optimum values to reach high separation efficiency (>99% separation of dye-linked albumin) were achieved for 60 nl/min and 50.0 V. Finally, Table VIII shows the studies on the separation of desired analytes based on ICP.

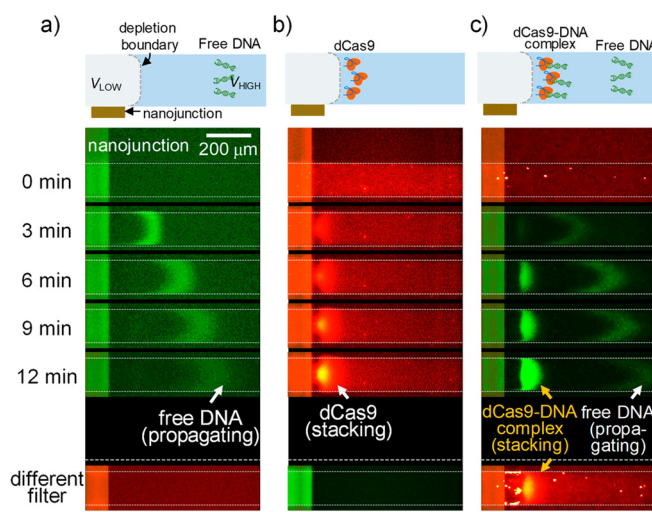


FIG. 14. Electrokinetic behaviors of (a) free DNA, (b) dCas9, and (c) dCas9-DNA complex. The electrophoretic mobilities were calculated as $1.34 \mu_{cr}$, $0.41 \mu_{cr}$, and $0.85 \mu_{cr}$, respectively, where $\mu_{cr} = 2.7 \times 10^{-8} \text{ m}^2/(\text{V s})$. Reprinted with permission from Lee *et al.*, *Nano Lett.* **18**, 7646 (2018). Copyright 2018 American Chemical Society.¹³⁰

TABLE VIII. Reported experiments with their operating conditions for separation process using ICP.

References	Microchannel	Nanojunction	Tracer	Tracer concentration	Voltage (V) or electric field	Separation resolution (SR) at time (min)
Song <i>et al.</i> ⁶⁴	PDMS	Nafion	Bound DNA	25 nM	80	1.85 at 4
Song <i>et al.</i> ¹²⁹	PDMS	BPE	Bound DNA	25 nM	80	1.5 at 4
Gong <i>et al.</i> ¹⁰⁶	Paper	Nafion	DNA	NR ^a	200 V/cm	0.7 at 1
Papadimitriou <i>et al.</i> ¹³⁴	PDMS	Nafion	PBS (phosphate buffered saline)	100 μ M	150	1.96 at 1
Choi <i>et al.</i> ⁶⁵	PDMS	Nafion	SRB	0.90 μ M	90	1.75 at 0.75
			Alexa Fluor 488	24.14 nM		

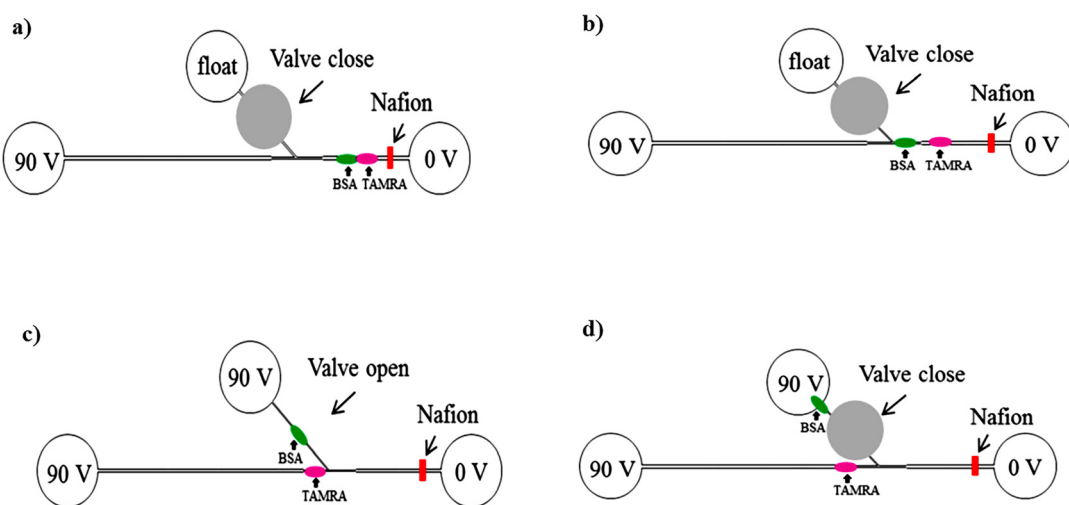
^aNR, not reported.

FIG. 15. Preconcentration, separation, guidance, and collection steps in a convergent microchannel with magnetic valve. (a) FITC-BSA and TAMRA are concentrated in horizontal microchannel. (b) FITC-BSA and TAMRA are separated in horizontal microchannel. (c) Magnetic valve is opened and guide FITC-BSA into separation microchannel. (d) FITC-BSA is collected in the reservoir and magnetic valve is closed to prevent backflow. Reproduced with permission from Biomicrofluidics **10**, 014119 (2016). Copyright 2016 AIP Publishing LLC.¹³³

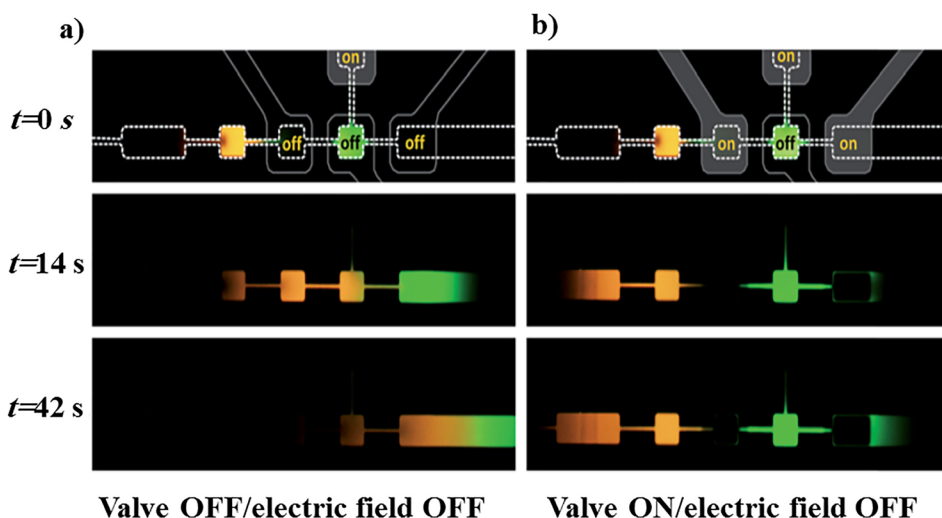


FIG. 16. A schematic of selective preconcentration and online collection of charged molecules by Choi *et al.*⁶⁵. Time-lapse images showing the dispersion of isolated plug when the valves were (a) OFF and (b) ON. Reproduced with permission from Choi *et al.*, RSC Adv. **5**, 66183 (2015). Copyright 2015 Royal Society of Chemistry.⁶⁵

Microvalves have been used to collect and direct the preconcentrated charged analytes to a certain position. Chiu *et al.*¹³³ improved their previous ICP-device with a convergent channel through adding an inclined channel (separation channel) with a magnetically actuated valve, Fig. 15. The mixed-species sample, FITC-BSA and TAMRA, was loaded into the main channel and a voltage difference of 90 V was applied to the concentrate sample while the valve was closed, Fig. 15(a). After the separation of FITC-BSA and TAMRA due to the difference in electrophoretic mobilities, Fig. 15(b), the valve was opened to direct the FITC-BSA into a separation channel, Fig. 15(c). This was achieved due to the faster movement of FITC-BSA than TAMRA. Then, the valve was closed to force TAMRA to pass through a horizontal channel, Fig. 15(d). A 50 and 90-fold enrichment factor for FITC-BSA and TAMRA was obtained within 720 s, respectively.

Choi *et al.*⁶⁵ employed pneumatic microvalves to selectively collect target analytes (SRB and Alexa Fluor 488) in an “H-shaped” micro/nanofluidic device with repeated microchamber, Figs. 16(a) and 16(b). The results revealed that Alexa dye could be preconcentrated up to 100-fold within approximately 40 s and then separated at a separation resolution of 1.75.

E. Integration of ICP with other devices

For detection of biomarkers in bodily fluids, it is desired to preconcentrate and detect low-abundance proteins or DNA molecules in a single chip. In this way, various attempts have been done to implement detection methods in ICP devices.

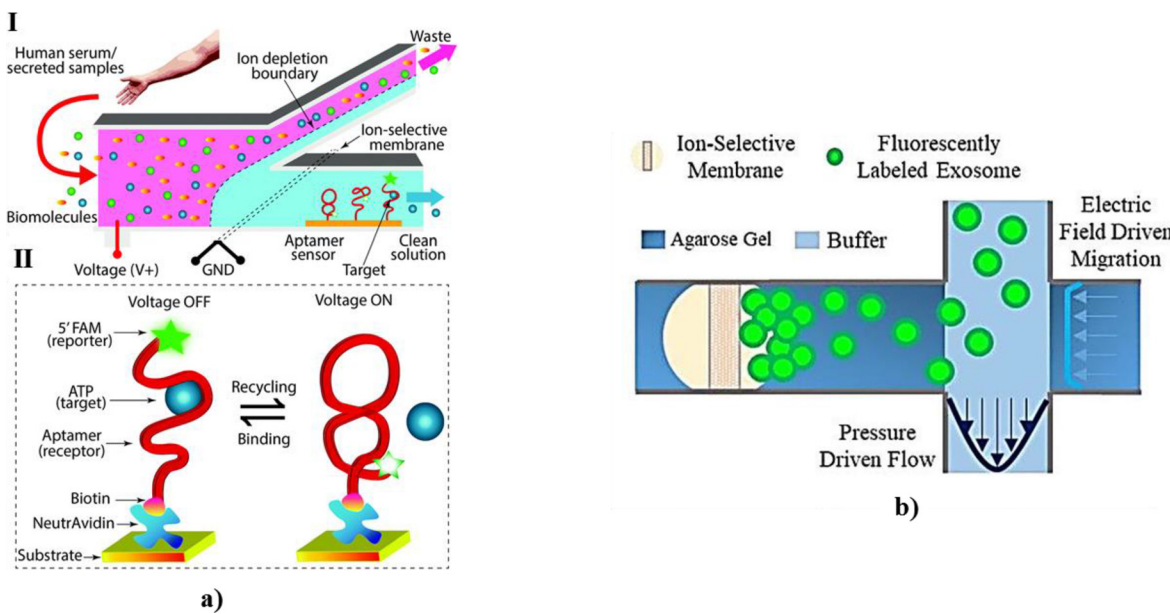


FIG. 17. (a) Schematic of the portable nanofluidic device for real-time target biomolecule monitoring, (I) biological samples were continuously uploaded to the device inlet for detection and subsequently converted to clean solution periodically for washing by applying an electric field across a Nafion® membrane. (II) The binding of the target biomolecule (i.e., ATP) to the aptamer immobilized on the glass substrate and the washing step are demonstrated. Reprinted with permission from Phan *et al.*, Lab Chip **18**, 575 (2018). Copyright 2018 Royal Society of Chemistry.³² (b) A zoomed view of the channels; as the exosomes pass through the intersection of the perpendicular channels, an electric field drives them into the gel where they concentrate at the membrane. Reprinted with permission from Marczak *et al.*, Electrophoresis **39**, 2029–2038 (2018). Copyright 2018 WILEY-VCH Verlag GmbH & Co. KGaA, Weinheim.¹³⁸

probe was incorporated in the ICP-based device. The MO probe and target DNA spiked into the human serum at 5×PBS by applying an external pressure of 100 Pa. The proposed device achieved an enrichment factor of >4800 with a detection limit for MO probe dropped to 3 pM within 15 min.

F. Cancer diagnosis

The exosomes are new biomarkers in extracellular vesicles used for early diagnosis of cancer. Marczak *et al.*¹³⁸ proposed an ICP device for simultaneous isolation and preconcentration of exosomes. As exosomes pass through the intersection of perpendicular channels, an electric field pulls exosomes into agarose gel toward the cation-selective membrane, Fig. 17(b). The device captures 70% of incoming exosomes from 1X PBS buffer, cell culture media, and blood serum at 150 μ l/h for at least 20 min.

Phan *et al.*^{91–94,137} proposed a Y-shaped ICP device for continuous measurement of the small biomolecules (e.g., adenosine triphosphate—ATP and cancer drug Doxorubicin—DOX) using aptamers, Fig. 17(a-I). Aptamers were used to bind with target biomolecules (i.e., ATP or DOX) to trigger a fluorescent signal for detecting targets in human serum. By triggering ICP, bound ATP molecules are removed from the ATP-aptamer complex and the mixed serum sample is turned into a clean solution within 5 min. The device exhibited a great ability to maintain fluorescent signals around 85% of the initial value of ATP after six detection cycles (2 h of continuous monitoring) Fig. 17(a-II).⁹²

Cheong *et al.*¹³⁹ proposed another strategy to detect and locally concentrate exosomes extracted from human breast cancer cell lines, MDA-MB-231, using SC-ICP. The device was able to concentrate exosomes (5.0×10^9 particles/ml) by almost 100-fold within 30 min.

VI. CONCLUSION AND FUTURE DIRECTIONS

In this paper, the concepts and fundamentals of the ICP phenomenon along with various configurations of ICP-based microdevices for preconcentrating applications were reviewed to provide insights for designing efficient ICP systems. Moreover, recent advances in the modification of device architecture for improving the efficiency of preconcentrating including parallelized sample channels, converging channels, microvalve implementation, simultaneous preconcentration, and separation, as well as the integration of ICP with sensors were discussed. Various active and passive methods for stabilizing the location of preconcentrated molecules and to control the location of the preconcentrated molecules in biological applications, desalination, and electrodialysis were discussed by analyzing their design considerations.

To increase the limit of detection for biological applications, ICP devices have been recently integrated with sensing modules. Future developments would be directed to the integration of miniaturized analytical devices with ICP-based microsystems. This allows for the fabrication of analytical methods with high design flexibility where compactness and portability are highly demanded. To realize such microsystems, high-performance ICP should be achieved using low electrical voltages with minimized power consumption. In addition, concentrated plugs should be highly focused in a fixed spot that could be detected using a miniaturized optical apparatus such as smartphones. Such ICP-based analytical devices would decrease the use of

laboratory equipment for rapid detection during an emergency and elderly care.

ACKNOWLEDGMENTS

S.A.M.S. acknowledges financial supports from National Institute for Medical Research Development (NIMAD) under Grant No. 957144 to conduct this project. A.K.M. acknowledges the receipt of R21-DC18818 from the National Institutes of Health.

DATA AVAILABILITY

The data that support the findings of this study are available from the corresponding author upon reasonable request.

REFERENCES

- ¹S. J. Kim, Y.-A. Song, and J. Han, “Nanofluidic concentration devices for biomolecules utilizing ion concentration polarization: Theory, fabrication, and applications,” *Chem. Soc. Rev.* **39**(3), 912–922 (2010).
- ²H. Cui *et al.*, “Isoelectric focusing in a poly (dimethylsiloxane) microfluidic chip,” *Anal. Chem.* **77**(5), 1303–1309 (2005).
- ³S. Song, A. K. Singh, and B. J. Kirby, “Electrophoretic concentration of proteins at laser-patterned nanoporous membranes in microchips,” *Anal. Chem.* **76**(15), 4589–4592 (2004).
- ⁴R. D. Oleschuk *et al.*, “Trapping of bead-based reagents within microfluidic systems: On-chip solid-phase extraction and electrochromatography,” *Anal. Chem.* **72**(3), 585–590 (2000).
- ⁵C.-C. Lin, J.-L. Hsu, and G.-B. Lee, “Sample preconcentration in microfluidic devices,” *Microfluid. Nanofluid.* **10**(3), 481–511 (2011).
- ⁶C. Zhao, Z. Ge, and C. Yang, “Microfluidic techniques for analytes concentration,” *Micromachines* **8**(1), 28 (2017).
- ⁷B. D. Storey *et al.*, “Electrokinetic instabilities in thin microchannels,” *Phys. Fluids* **17**(1), 018103 (2005).
- ⁸D. Yan *et al.*, “Diagnosis of transient electrokinetic flow in microfluidic channels,” *Phys. Fluids* **19**(1), 017114 (2007).
- ⁹A. J. Moghadam, “Unsteady electrokinetic flow in a Microcapillary: Effects of periodic excitation and geometry,” *J. Fluids Eng.* **141**, 111104 (2019).
- ¹⁰R. B. Schoch, H. Van Lintel, and P. Renaud, “Effect of the surface charge on ion transport through nanoslits,” *Phys. Fluids* **17**(10), 100604 (2005).
- ¹¹T. Kim and E. Meyhöfer, “Nanofluidic concentration of selectively extracted biomolecule analytes by microtubules,” *Anal. Chem.* **80**(14), 5383–5390 (2008).
- ¹²S. H. Ko *et al.*, “Nanofluidic preconcentration device in a straight microchannel using ion concentration polarization,” *Lab Chip* **12**(21), 4472–4482 (2012).
- ¹³C. J. Striemer *et al.*, “Charge-and size-based separation of macromolecules using ultrathin silicon membranes,” *Nature* **445**(7129), 749–753 (2007).
- ¹⁴B. Ma, J. Chi, and H. Liu, “Fabric-based ion concentration polarization for pump-free water desalination,” *ACS Sustainable Chem. Eng.* **6**(1), 99–103 (2018).
- ¹⁵D.-T. Phan, *et al.*, “Sample concentration in a microfluidic paper-based analytical device using ion concentration polarization,” *Sens. Actuators, B* **222**, 735–740 (2016).
- ¹⁶R. Kwak G. F. Guan, W. K. Peng, and J. Y. Han, “Microscale electrodialysis: Concentration profiling and vortex visualization,” *Desalination* **308**, 138–146 (2014).
- ¹⁷B. D. MacDonald *et al.*, “Out-of-plane ion concentration polarization for scalable water desalination,” *Lab Chip* **14**(4), 681–685 (2014).
- ¹⁸S. J. Kim *et al.*, “Direct seawater desalination by ion concentration polarization,” *Nat. Nanotechnol.* **5**(4), 297–301 (2010).
- ¹⁹W. Liu *et al.*, “A universal design of field-effect-tunable microfluidic ion diode based on a gating cation-exchange nanoporous membrane,” *Phys. Fluids* **29**(11), 112001 (2017).
- ²⁰R. Yan *et al.*, “Nanofluidic diodes based on nanotube heterojunctions,” *Nano Lett.* **9**(11), 3820–3825 (2009).

- ²¹H. Daiguji, Y. Oka, and K. Shirono, "Nanofluidic diode and bipolar transistor," *Nano Lett.* **5**(11), 2274–2280 (2005).
- ²²D. Kim *et al.*, "Non-equilibrium electrokinetic micro/nano fluidic mixer," *Lab Chip* **8**(4), 625–628 (2008).
- ²³O. Jännig and N.-T. Nguyen, "A polymeric high-throughput pressure-driven micromixer using a nanoporous membrane," *Microfluid. Nanofluid.* **10**(3), 513–519 (2011).
- ²⁴A. S. Khair, "Concentration polarization and second-kind electrokinetic instability at an ion-selective surface admitting normal flow," *Phys. Fluids* **23**(7), 072003 (2011).
- ²⁵C. P. Nielsen and H. Bruus, "Transport-limited water splitting at ion-selective interfaces during concentration polarization," *Phys. Rev. E* **89**(4), 042405 (2014).
- ²⁶V. Zabolotsky *et al.*, "Coupled transport phenomena in overlimiting current electrodialysis," *Sep. Purif. Technol.* **14**(1–3), 255–267 (1998).
- ²⁷E. V. Dydek *et al.*, "Overlimiting current in a microchannel," *Phys. Rev. Lett.* **107**(11), 118301 (2011).
- ²⁸I. Rubinstein and B. Zaltzman, "Equilibrium electroconvective instability," *Phys. Rev. Lett.* **114**(11), 114502 (2015).
- ²⁹C. Druzgalski, M. Andersen, and A. Mani, "Direct numerical simulation of electroconvective instability and hydrodynamic chaos near an ion-selective surface," *Phys. Fluids* **25**(11), 110804 (2013).
- ³⁰S. J. Kim *et al.*, "Multi-vortical flow inducing electrokinetic instability in ion concentration polarization layer," *Nanoscale* **4**(23), 7406–7410 (2012).
- ³¹M. H. Oddy and J. G. Santiago, "Multiple-species model for electrokinetic instability," *Phys. Fluids* **17**(6), 064108 (2005).
- ³²Z. Li *et al.*, "Accurate multi-physics numerical analysis of particle preconcentration based on ion concentration polarization," *Int. J. Appl. Mech.* **09**(08), 1750107 (2017).
- ³³M. Jia and T. Kim, "Multiphysics simulation of ion concentration polarization induced by a surface-patterned nanoporous membrane in single channel devices," *Anal. Chem.* **86**(20), 10365–10372 (2014).
- ³⁴M. Jia and T. Kim, "Multiphysics simulation of ion concentration polarization induced by nanoporous membranes in dual channel devices," *Anal. Chem.* **86**(15), 7360–7367 (2014).
- ³⁵A. N. Chatterjee *et al.*, "Modeling and simulation of ionic currents in three-dimensional microfluidic devices with nanofluidic interconnects," *J. Nanopart. Res.* **7**(4–5), 507–516 (2005).
- ³⁶A. N. Chatterjee and N. Aluru, "Combined circuit/device modeling and simulation of integrated microfluidic systems," *J. Microelectromech. Syst.* **14**(1), 81–95 (2005).
- ³⁷K.-B. Sung *et al.*, "Development of a nanofluidic preconcentrator with precise sample positioning and multi-channel preconcentration," *Microfluid. Nanofluid.* **14**(3–4), 645–655 (2013).
- ³⁸C. Duan, W. Wang, and Q. Xie, "Fabrication of nanofluidic devices," *Biomicrofluidics* **7**(2), 026501 (2013).
- ³⁹A. W. Martinez *et al.*, "Diagnostics for the developing world: Microfluidic paper-based analytical devices," *Anal. Chem.* **82**(1), 3–10 (2010).
- ⁴⁰A. Perera *et al.*, "Enhanced sample pre-concentration by ion concentration polarization on a paraffin coated converging microfluidic paper based analytical platform," *Biomicrofluidics* **14**(1), 014103 (2020).
- ⁴¹N. Liu, D.-T. Phan, and W. S. Lew, "An enclosed paper microfluidic chip as a sample preconcentrator based on ion concentration polarization," *IEEE Trans. Biomed. Circuits Syst.* **11**(6), 1392–1399 (2017).
- ⁴²N. Liu *et al.*, "Direct spraying method for fabrication of paper-based microfluidic devices," *J. Micromech. Microeng.* **27**(10), 104001 (2017).
- ⁴³V. Leung *et al.*, "Streaming potential sensing in paper-based microfluidic channels," *Colloids Surf., A* **364**(1–3), 16–18 (2010).
- ⁴⁴S. J. Kim *et al.*, "Concentration Polarization and nonlinear electrokinetic flow near a nanofluidic channel," *Phys. Rev. Lett.* **99**(4), 044501 (2007).
- ⁴⁵S. Y. Son, H. Lee, and S. J. Kim, "Paper-based ion concentration polarization device for selective preconcentration of muc1 and lamp-2 genes," *Micro Nano Syst. Lett.* **5**(1), 8 (2017).
- ⁴⁶P. Mao and J. Han, "Fabrication, and characterization of 20 nm planar nanofluidic channels by glass–glass and glass–silicon bonding," *Lab Chip* **5**(8), 837–844 (2005).
- ⁴⁷P. Mao and J. Han, "Massively-parallel ultra-high-aspect-ratio nanochannels as mesoporous membranes," *Lab Chip* **9**(4), 586–591 (2009).
- ⁴⁸C. C. Chang, C. P. Yeh, and R. J. Yang, "Ion concentration polarization near microchannel-nanochannel interfaces: Effect of pH value," *Electrophoresis* **33**(5), 758–764 (2012).
- ⁴⁹S. M. Kim, M. A. Burns, and E. F. Hasselbrink, "Electrokinetic protein pre-concentration using a simple glass/poly(dimethylsiloxane) microfluidic chip," *Anal. Chem.* **78**(14), 4779–4785 (2006).
- ⁵⁰J. H. Lee, Y.-A. Song, and J. Han, "Multiplexed proteomic sample preconcentration device using surface-patterned ion-selective membrane," *Lab Chip* **8**(4), 596–601 (2008).
- ⁵¹S. J. Kim and J. Han, "Self-sealed vertical polymeric nanoporous-junctions for high-throughput nanofluidic applications," *Anal. Chem.* **80**(9), 3507–3511 (2008).
- ⁵²D. Das *et al.*, "A multi-module microfluidic platform for continuous pre-concentration of water-soluble ions and separation of oil droplets from oil-in-water (O/W) emulsions using a DC-biased AC electrokinetic technique," *Electrophoresis* **38**, 645–652 (2017).
- ⁵³D.-T. Phan, C. Yang, and N.-T. Nguyen, "A continuous-flow droplet-based concentrator using ion concentration polarization," *RSC Adv.* **5**, 44336–44341 (2015).
- ⁵⁴D.-T. Phan, *et al.*, "Real-time ATP monitoring in human serum by an nanofluidic device integrated with an aptamer sensor," in *The 7th International Multidisciplinary Conference on Optofluidics 2017 (Optofluidics)* (MDPI, 2017).
- ⁵⁵D.-T. Phan, "Ion concentration polarization and its application," Doctoral thesis (Nanyang Technological University, Singapore, 2016).
- ⁵⁶R. Kwak *et al.*, "Enhanced salt removal by unipolar ion conduction in ion concentration polarization desalination," *Sci. Rep.* **6**(1), 25349 (2016).
- ⁵⁷B. Kim *et al.*, "Purification of high salinity brine by multi-stage ion concentration polarization desalination," *Sci. Rep.* **6**(1), 31850 (2016).
- ⁵⁸M. Li and R. K. Anand, "Recent advancements in ion concentration polarization," *Analyst* **141**(12), 3496–3510 (2016).
- ⁵⁹S. Y. Son *et al.*, "Engineered nanofluidic preconcentration devices by ion concentration polarization," *BioChip J.* **10**(4), 251–261 (2016).
- ⁶⁰Y.-C. Wang, A. L. Stevens, and J. Han, "Million-fold preconcentration of proteins and peptides by nanofluidic filter," *Anal. Chem.* **77**(14), 4293–4299 (2005).
- ⁶¹B. Kim *et al.*, "Tunable ionic transport for a triangular nanochannel in a polymeric nanofluidic system," *ACS Nano* **7**(1), 740–747 (2013).
- ⁶²A.-C. Louér, *et al.*, "Pressure-assisted selective preconcentration in a straight nanochannel," *Anal. Chem.* **85**(16), 7948–7956 (2013).
- ⁶³P.-S. Chung *et al.*, "Real-time dual-loop electric current measurement for label-free nanofluidic preconcentration chip," *Lab Chip* **15**(1), 319–330 (2015).
- ⁶⁴H. Song *et al.*, "Nafion-film-based micro-nanofluidic device for concurrent DNA preconcentration and separation in free solution," *Microfluid. Nanofluid.* **17**(4), 693–699 (2014).
- ⁶⁵J. Choi *et al.*, "Selective preconcentration and online collection of charged molecules using ion concentration polarization," *RSC Adv.* **5**(81), 66178–66184 (2015).
- ⁶⁶S. Nam *et al.*, "Experimental verification of overlimiting current by surface conduction and electro-osmotic flow in microchannels," *Phys. Rev. Lett.* **114**(11), 114501 (2015).
- ⁶⁷L. Gong *et al.*, "Force fields of charged particles in micro-nanofluidic preconcentration systems," *AIP Adv.* **7**(12), 125020 (2017).
- ⁶⁸S. A. Hong *et al.*, "Electrochemical detection of methylated DNA on a microfluidic chip with nanoelectrokinetic pre-concentration," *Biosens. Bioelectron.* **107**, 103–110 (2018).
- ⁶⁹S.-M. Ngom *et al.*, "Electropreconcentration diagrams to optimize molecular enrichment with low counter pressure in a nanofluidic device," *Electrophoresis* **41**, 1617 (2020).
- ⁷⁰M. Gholinejad *et al.*, "Multifactorial analysis of ion concentration polarization for microfluidic preconcentrating applications using response surface method," *Phys. Fluids* **32**(7), 072012 (2020).
- ⁷¹X. Yuan *et al.*, "Electrokinetic biomolecule preconcentration using xurography-based micro-nano-micro fluidic devices," *Anal. Chem.* **87**(17), 8695–8701 (2015).

- ⁷²P. Hailong *et al.*, “3D printed micro/nanofluidic preconcentrator for charged sample based on ion concentration polarization,” *J. Micromech. Microeng.* **27**(5), 055008 (2017).
- ⁷³M. Kim, M. Jia, and T. Kim, “Ion concentration polarization in a single and open microchannel induced by a surface-patterned perm-selective film,” *Analyst* **138**(5), 1370–1378 (2013).
- ⁷⁴H. Yu *et al.*, “A simple, disposable microfluidic device for rapid protein concentration and purification via direct-printing,” *Lab Chip* **8**(9), 1496–1501 (2008).
- ⁷⁵M. Shen *et al.*, “Microfluidic protein preconcentrator using a microchannel-integrated Nafion strip: Experiment and modeling,” *Anal. Chem.* **82**(24), 9989–9997 (2010).
- ⁷⁶M. Kim and T. Kim, “Integration of nanoporous membranes into microfluidic devices: Electrokinetic bio-sample pre-concentration,” *Analyst* **138**(20), 6007–6013 (2013).
- ⁷⁷S. J. Kim, L. D. Li, and J. Han, “Amplified electrokinetic response by concentration polarization near nanofluidic channel,” *Langmuir* **25**(13), 7759–7765 (2009).
- ⁷⁸Y.-C. Wang and J. Han, “Pre-binding dynamic range and sensitivity enhancement for immuno-sensors using nanofluidic preconcentrator,” *Lab Chip* **8**(3), 392–394 (2008).
- ⁷⁹J. Dai *et al.*, “Electrokinetic trapping and concentration enrichment of DNA in a microfluidic channel,” *J. Am. Chem. Soc.* **125**(43), 13026–13027 (2003).
- ⁸⁰R. S. Foote *et al.*, “Preconcentration of proteins on microfluidic devices using porous silica membranes,” *Anal. Chem.* **77**(1), 57–63 (2005).
- ⁸¹H. Chun, T. D. Chung, and J. M. Ramsey, “High yield sample preconcentration using a highly ion-conductive charge-selective polymer,” *Anal. Chem.* **82**(14), 6287–6292 (2010).
- ⁸²C.-P. Jen *et al.*, “Protein preconcentration using nanofractures generated by nanoparticle-assisted electric breakdown at junction gaps,” *PLoS One* **9**(7), e102050 (2014).
- ⁸³A. Syed *et al.*, “Creating sub-50 nm nanofluidic junctions in a PDMS microchip via self-assembly process of colloidal silica beads for electrokinetic concentration of biomolecules,” *Lab Chip* **14**(23), 4455–4460 (2014).
- ⁸⁴W. Ouyang *et al.*, “Deciphering ion concentration polarization-based electrokinetic molecular concentration at the micro-nanofluidic interface: Theoretical limits and scaling laws,” *Nanoscale* **10**(32), 15187–15194 (2018).
- ⁸⁵B. Scarff, C. Escobedo, and D. Sinton, “Radial sample preconcentration,” *Lab Chip* **11**(6), 1102–1109 (2011).
- ⁸⁶K. Aizel *et al.*, “Investigation of ion concentration polarization in original micro-nanofluidic devices,” *Procedia Eng.* **47**, 269–272 (2012).
- ⁸⁷K. Aizel, Y. Fouillet, and C. Pudda, “Electropreconcentration of nanoparticles using a radial micro-nanofluidic device,” *J. Nanopart. Res.* **16**(11), 2731 (2014).
- ⁸⁸M. M. Gong *et al.*, “Nanoporous membranes enable concentration and transport in fully wet paper-based assays,” *Anal. Chem.* **86**(16), 8090–8097 (2014).
- ⁸⁹S. Lee *et al.*, “Nanoelectrokinetic bufferchannel-less radial preconcentrator and online extractor by tunable ion depletion layer,” *Biomicrofluidics* **13**(3), 034113 (2019).
- ⁹⁰S. Lee *et al.*, “Nanoelectrokinetic radial preconcentrator/extractor based on ion concentration polarization,” in *2017 IEEE 30th International Conference on Micro Electro Mechanical Systems (MEMS)* (IEEE, 2017).
- ⁹¹D.-T. Phan *et al.*, “Buffer-free continuous-flow biosensors for real-time monitoring of small biomolecules in human biofluids by ion concentration polarization,” in *22nd International Conference on Miniaturized Systems for Chemistry and Life Sciences (MicroTAS 2018)* (Chemical and Biological Microsystems Society, 2018).
- ⁹²D.-T. Phan *et al.*, “Buffer-free integrative nanofluidic device for real-time continuous flow bioassays by ion concentration polarization,” *Lab Chip* **18**(4), 574–584 (2018).
- ⁹³D.-T. Phan *et al.*, “Real-time ATP monitoring in human serum by a nanofluidic device integrated with an aptamer sensor,” in *21st International Conference on Miniaturized Systems for Chemistry and Life Sciences (MicroTAS 2017)* (Chemical and Biological Microsystems Society, 2017), pp. 203–204.
- ⁹⁴L. Jin *et al.*, “An auto-regeneratable electrochemical aptasensor for continuous monitoring of biomolecules enabled by ion concentration polarization,” in *21st International Conference on Miniaturized Systems for Chemistry and Life Sciences (MicroTAS 2017)* (Chemical and Biological Microsystems Society, 2017).
- ⁹⁵D.-T. Phan, C. Yang, and N.-T. Nguyen, “Fabrication of nanoporous junctions using off-the-shelf Nafion membrane,” *J. Micromech. Microeng.* **25**(11), 115019 (2015).
- ⁹⁶S. Hong, R. Kwak, and W. Kim, “based flow fractionation system applicable to preconcentration and field-flow separation,” *Anal. Chem.* **88**(3), 1682–1687 (2016).
- ⁹⁷B. Berzina and R. K. Anand, “An electrokinetic separation route to source dialysate from excess fluid in blood,” *Anal. Chem.* **90**(6), 3720–3726 (2018).
- ⁹⁸R. Kwak, S. J. Kim, and J. Han, “Continuous-flow biomolecule and cell concentrator by ion concentration polarization,” *Anal. Chem.* **83**(19), 7348–7355 (2011).
- ⁹⁹S. H. Ko *et al.*, “Massively parallel concentration device for multiplexed immunoassays,” *Lab Chip* **11**(7), 1351–1358 (2011).
- ¹⁰⁰C. L. Chen and R. J. Yang, “Effects of microchannel geometry on preconcentration intensity in microfluidic chips with straight or convergent-divergent microchannels,” *Electrophoresis* **33**(5), 751–757 (2012).
- ¹⁰¹C.-C. Chao, P.-H. Chiu, and R.-J. Yang, “Preconcentration of diluted biochemical samples using microchannel with integrated nanoscale Nafion membrane,” *Biomed. Microdevices* **17**(2), 25 (2015).
- ¹⁰²X. Wei *et al.*, “Increasing the detection sensitivity for DNA-morpholino hybridization in sub-nanomolar regime by enhancing the surface ion conductance of PEDOT: PSS membrane in a microchannel,” *ACS Sens.* **1**(7), 862–865 (2016).
- ¹⁰³C.-H. Chang and R.-J. Yang, “Enhanced sample preconcentration in microfluidic chip using graphene oxide-Nafion membrane,” *Microfluid. Nanofluid.* **20**(12), 168 (2016).
- ¹⁰⁴R. Dhopeshwarkar *et al.*, “Transient effects on microchannel electrokinetic filtering with an ion-permselective membrane,” *Anal. Chem.* **80**(4), 1039–1048 (2008).
- ¹⁰⁵J. Quist *et al.*, “Elastomeric microvalves as tunable nanochannels for concentration polarization,” *Lab Chip* **13**(24), 4810–4815 (2013).
- ¹⁰⁶M. G. Gong *et al.*, “Direct DNA analysis with paper-based ion concentration polarization,” *J. Am. Chem. Soc.* **137**(43), 13913–13919 (2015).
- ¹⁰⁷R.-J. Yang, H.-H. Pu, and H.-L. Wang, “Ion concentration polarization on paper-based microfluidic devices and its application to preconcentrate dilute sample solutions,” *Biomicrofluidics* **9**(1), 014122 (2015).
- ¹⁰⁸R. Kwak, J. Y. Kang, and T. S. Kim, “Spatiotemporally defining biomolecule preconcentration by merging ion concentration polarization,” *Anal. Chem.* **88**(1), 988–996 (2016).
- ¹⁰⁹S.-H. Yeh, K.-H. Chou, and R.-J. Yang, “Sample pre-concentration with high enrichment factors at a fixed location in paper-based microfluidic devices,” *Lab Chip* **16**(5), 925–931 (2016).
- ¹¹⁰S. J. Lee *et al.*, “Preconcentration of lipid vesicles using concentration polarization in a microfluidic chip,” *Sens. Actuators, B* **229**, 276–280 (2016).
- ¹¹¹Q. Liu, C. Xu, and H. Liang, “Laser carved micro-crack channels in paper-based dilution devices,” *Talanta* **175**, 289–296 (2017).
- ¹¹²H. Gao *et al.*, “Electrokinetic stacking on paper-based analytical device by ion concentration polarization with ion exchange membrane interface,” *Microfluid. Nanofluid.* **22**(5), 50 (2018).
- ¹¹³A. Perera *et al.*, “Rapid pre-concentration of *Escherichia coli* in a microfluidic paper-based device using ion concentration polarization,” *Electrophoresis* **41**(10–11), 867–874 (2020).
- ¹¹⁴L. F. Cheow *et al.*, “Increasing the sensitivity of enzyme-linked immunosorbent assay using multiplexed electrokinetic concentrator,” *Anal. Chem.* **82**(8), 3383–3388 (2010).
- ¹¹⁵W. Ouyang, Z. Li, and J. Han, “Pressure-modulated selective electrokinetic trapping for direct enrichment, purification, and detection of nucleic acids in human serum,” *Anal. Chem.* **90**(19), 11366–11375 (2018).
- ¹¹⁶P.-H. Chiu, C.-H. Weng, and R.-J. Yang, “Preconcentration and separation of mixed-species samples near a nano-junction in a convergent microchannel,” *Sensors* **15**(12), 30704–30715 (2015).
- ¹¹⁷P. Kovář, D. Tichý, and Z. Slouka, “Effect of channel geometry on ion-concentration polarization-based preconcentration and desalination,” *Biomicrofluidics* **13**(6), 064102 (2019).

- ¹¹⁸Y. T. Atalay *et al.*, “Modeling and optimization of a multi-enzyme electrokinetically driven multiplexed microchip for simultaneous detection of sugars,” *Microfluid. Nanofluid.* **7**(3), 393 (2009).
- ¹¹⁹L. Li and D. Kim, “Propagating behavior comparison of analytes and background electrolytes in a concentration polarization process,” *BioChip J.* **11**(2), 121–130 (2017).
- ¹²⁰Q. Yu and Z. Silber-Li, “Measurements of the ion-depletion zone evolution in a micro/nano-channel,” *Microfluid. Nanofluid.* **11**(5), 623–631 (2011).
- ¹²¹T. A. Zangle, A. Mani, and J. G. Santiago, “On the propagation of concentration polarization from microchannel–nanochannel interfaces Part II: Numerical and experimental study,” *Langmuir* **25**(6), 3909–3916 (2009).
- ¹²²A. Mani, T. A. Zangle, and J. G. Santiago, “On the propagation of concentration polarization from microchannel–nanochannel interfaces Part I: Analytical model and characteristic analysis,” *Langmuir* **25**(6), 3898–3908 (2009).
- ¹²³J. Kim *et al.*, “Ion concentration polarization by bifurcated current path,” *Sci. Rep.* **7**(1), 5091 (2017).
- ¹²⁴K. Kim *et al.*, “Stabilization of ion concentration polarization layer using micro fin structure for high-throughput applications,” *Nanoscale* **9**(10), 3466–3475 (2017).
- ¹²⁵S. J. Lee, J. Lee, and K. Kim, “Pressure-driven spontaneous ion concentration polarization using an ion-selective membrane,” *Anal. Biochem.* **557**, 13–17 (2018).
- ¹²⁶D.-T. Phan and N.-T. Nguyen, “Self-triggering regime for synchronized formation of two droplets,” *Appl. Phys. Lett.* **104**(8), 084104 (2014).
- ¹²⁷S. Park and G. Yossifon, “Electrothermal based active control of ion transport in a microfluidic device with an ion-permselective membrane,” *Nanoscale* **10**(24), 11633–11641 (2018).
- ¹²⁸Z.-Y. Wu *et al.*, “Simultaneous electrokinetic concentration and separation of proteins on a paper-based analytical device,” *RSC Adv.* **7**(7), 4011–4016 (2017).
- ¹²⁹H. Song *et al.*, “Concurrent DNA preconcentration and separation in bipolar electrode-based microfluidic device,” *Anal. Methods* **7**(4), 1273–1279 (2015).
- ¹³⁰H. Lee *et al.*, “dCas9-mediated nanoelectrokinetic direct detection of target gene for liquid biopsy,” *Nano Lett.* **18**(12), 7642–7650 (2018).
- ¹³¹S. Baek *et al.*, “Dynamics of driftless preconcentration using ion concentration polarization leveraged by convection and diffusion,” *Lab Chip* **19**(19), 3190–3199 (2019).
- ¹³²J. Choi *et al.*, “Nanoelectrokinetic selective preconcentration based on ion concentration polarization,” *BioChip J.* **14**(1), 100–109 (2020).
- ¹³³Y.-Y. Chen *et al.*, “Preconcentration of diluted mixed-species samples following separation and collection in a micro-nanofluidic device,” *Biomicrofluidics* **10**(1), 014119 (2016).
- ¹³⁴V. A. Papadimitriou, L. I. Segerink, and J. C. Eijkel, “Free flow ion concentration polarization focusing (FF-ICPF),” *Anal. Chem.* **92**(7), 4866–4874 (2020).
- ¹³⁵V. Subramanian *et al.*, “Enhancing the sensitivity of point-of-use electrochemical microfluidic sensors by ion concentration polarisation—A case study on arsenic,” *Sens. Actuators, B* **304**, 127340 (2020).
- ¹³⁶C. Wang *et al.*, “Ultrasensitive protein concentration detection on a micro/nanofluidic enrichment chip using fluorescence quenching,” *ACS Appl. Mater. Interfaces* **7**(12), 6835–6841 (2015).
- ¹³⁷D.-T. Phan *et al.*, “Integrative wireless device for remote continuous blood biomarker monitoring,” in 24th International Conference on Miniaturized Systems for Chemistry and Life Sciences (MicroTAS, 2020) (2020).
- ¹³⁸S. Marczak *et al.*, “Simultaneous isolation and preconcentration of exosomes by ion concentration polarization,” *Electrophoresis* **39**(15), 2029–2038 (2018).
- ¹³⁹L. S. Cheung *et al.*, “Rapid detection and trapping of extracellular vesicles by electrokinetic concentration for liquid biopsy on chip,” *Micromachines* **9**(6), 306 (2018).